Fast and Stable Schemes for Phase Fields Models

Matthieu Brachet, Jean-Paul Chehab

Fast and Stable Schemes for Phase Fields Models

March 23, 2020

Matthieu Brachet[1] and Jean-Paul Chehab[2]

[1]Laboratoire LJK (UMR CNRS 5224) and INRIA Project AIRSEA- Bâtiment IMAG, Université Grenoble Alpes
700 Avenue Centrale, Campus de Saint Martin d'Hères
38401 Domaine Universitaire de Saint-Martin-d'Hères
matthieu.brachet@inria.fr

[2]Laboratoire LAMFA (UMR CNRS 7352), Université de Picardie Jules Verne
33 rue Saint Leu, 80039 Amiens Cédex, France
Jean-Paul.Chehab@u-picardie.fr

Abstract

We propose and analyse new stabilized time marching schemes for Phase Fields model such as Allen-Cahn and Cahn-Hillard equations, when discretized in space with high order finite differences compact schemes. The stabilization applies to semi-implicit schemes for which the linear part is simplified using sparse pre-conditioners. The new methods allow to significant obtain a gain of CPU time. The numerical illustrations we give concern applications on pattern dynamics and on image processing (inpainting, segmentation) in two and three dimension cases.

Keywords: Allen-Cahn equation, Cahn-Hilliard equation, finite differences, compact schemes, preconditioning, stability
AMS Classification[2010]: 35K57, 65F08, 65L20, 65M06

1 Introduction

Diffuse interface dynamics governed by Phase fields equations, such as Allen-Cahn's or Cahn-Hilliard's, play an important role in a large number of applications: let us cite [2, 3, 19, 31] in material science, [5, 6, 7, 21, 24, 26, 27] in image processing, [26, 30] in chemistry [10, 22] or in ecology and in medicine, the list being non-exhaustive. In addition, the interest for these models in the mathematical analysis point of view is considerably developed since the last three decades, notably in the study of the long time behavior of the solutions, see e.g. [17, 18, 37], making the simulation of Phase fields models a key issue.

The numerical integration of such reaction-diffusion equations can be a delicate task: it needs to recover at the discrete level intrinsic properties of the solution (Energy diminishing, maximum principle) and the presence of small parameter $\epsilon > 0$ (typically, the interphase length) can generate practical difficulties in the iterations processes with a hard time step restriction, even for fully-implicit schemes ; this is due on the way the fixed points problems are solved at each iteration.

The construction of a robust (stable) and efficient (fast) scheme lies on the balance between the advantages and the drawbacks of implicit (stable but costly) and of explicit (fast but with often hard stability condition) times-marching schemes. For instance, the simple Forward Euler's, can be used only

for small time steps; this restriction can be very important, e.g., when considering heat-equation, the basic linear part of reaction-diffusion equations. This restriction allows to prevent the expansion of high mode components, the ones that lead to the divergence of the scheme. A way to enhance the stability region while solving a relatively simple linear system is to introduce a proper approximation to an unconditionally stable scheme. Consider, e.g., Backward Euler's applied to the discretized Heat equation:

$$\frac{u^{(k+1)}-u^{(k)}}{\Delta t}+Au^{(k+1)}=0, \tag{1}$$

where A is the stiffness matrix, $\Delta t>0$, the time step; here $u^{(k)}$ is the approximation of the solution at time $t=k\Delta t$ in the spatial approximation space. To simplify the linear system that must be solved at each step, one replaces $Au^{(k+1)}$ by $\tau B(u^{(k+1)}-u^{(k)})+Au^{(k)}$, where $\tau\geq 0$ and where B is a pre-conditioner of A; the new scheme reads as

$$\frac{u^{(k+1)}-u^{(k)}}{\Delta t}+\tau B(u^{(k+1)}-u^{(k)})+Au^{(k)}=0. \tag{2}$$

This stabilization procedure, also called RSS scheme (Residual Smoothing Scheme), was introduced independently by [4] and [12] (in the multilevel case), see also [8] for recent developments. It allows to take large time steps while simplifying the linear problem to solve at each step: in that way the stability is enhanced and in addition a save of computation time can be obtained as respect to the classical backward Euler's scheme. Of course there exist many different stabilization procedures that can be applied to a large variety of schemes used for reaction-diffusion equations, see, e.g. [15, 16], particularly those based on hyperbolic perturbations that we will not consider here. The stabilized scheme for a reaction-diffusion equation writes as

$$\frac{u^{(k+1)}-u^{(k)}}{\Delta t}+\tau B(u^{(k+1)}-u^{(k)})+Au^{(k)}+f(u^{(k)})=0. \tag{3}$$

It corresponds to a stabilized semi-implicit Euler scheme for, e.g., Allen-Cahn equations; in the same way, using the stabilization procedure, we can consider coupled systems as

$$\frac{u^{(k+1)}-u^{(k)}}{\Delta t}+\tau B(\mu^{(k+1)}-\mu^{(k)})+A\mu^{(k)}=0, \tag{4}$$

$$\mu^{(k+1)}=\tau B(u^{(k+1)}-u^{(k)})+Au^{(k)}+f(u^{(k)})=0. \tag{5}$$

The technique can then applied to high order or coupled problems such as Cahn-Hilliard's. It must be noticed that this stabilization procedure allows to recover the same steady states as the original scheme, this is an important property when considering, e.g., inpainting or image segmentation problems.

The aim of this article is to propose and analyze fast finite differences schemes for phase fields with a focus on Allen-Cahn and Cahn-Hilliard equations, when the space discretization is realized with finite differences compact schemes. The new methods combine high order compact finite differences schemes for the discretization in space together with a stabilization of explicit time schemes implemented by using low coast pre-conditioners of the linear term.

The article is organized as follows: in Section 2 we consider the linear case, we recall the principle of the stabilization (RSS- scheme) and derive stability results for a number of time schemes that will be used in the non linear case. After that, in Section 3, then in Section 4, we introduce and study new stabilized schemes for Allen-Cahn's (then Cahn-Hilliard's) equation. We give in particular conditions to obtain energy diminishing schemes. In Section 5 we present numerical illustrations on pattern dynamics, image segmentation and inpainting.

2 Stabilized schemes in the linear case

We first give here stability results for stabilized-Schemes derived from time marching method in the linear case; these schemes will be used to build new methods for solving nonlinear time dependent problems, as presented in Sections 3 and 4.

2.1 Explicit Schemes and stabilization

Consider the Heat equation

$$\frac{\partial u}{\partial t} - \Delta u = 0, \quad x \in \Omega,\ t > 0, \tag{6}$$

$$u = 0 \quad x \in \partial\Omega, t > 0, \tag{7}$$

$$u(x,0) = u_0(x) \qquad x \in \Omega. \tag{8}$$

They are several ways to express the stability of a scheme, depending on the norm one considers to measure the boundedness of the sequence of time approximations of the solution. We will focus on two following stability notions

- Stability in Energy (a consequence of energy time-diminishing):

$$\sum_{|\alpha|=0}^{m} \aleph_\alpha \|D^\alpha u(t)\|^2_{L^2\Omega)} \leq \sum_{|\alpha|=0}^{m} \aleph_\alpha \|D^\alpha u(t')\|^2_{L^2\Omega)},\ \forall t > t',$$

  with $\aleph_\alpha \geq 0,\ \sum \aleph_\alpha > 0$.

- L^∞ Stability (a consequence of the maximum principle):

$$\exists L > 0 / \|u(t)\|_{L^\infty} \leq L, \forall t \geq 0.$$

The space discretization of (6) leads to the differential system

$$\frac{du}{dt} + Au = 0, \quad x \in \Omega,\ t > 0, \tag{9}$$

$$u(0) = u_0. \tag{10}$$

Here A is the stiffness matrix. The time numerical integration of (9) produces a sequence of vectors $u^{(k)} \simeq u(k\Delta t)$, and we define the stability of the schemes as

- Stability in Energy (discrete Energy diminishing), e.g.,

$$\frac{1}{2} < Au^{(k+1)}, u^{(k+1)} > \leq \frac{1}{2} < Au^{(k)}, u^{(k)} >, \forall k \geq 0,$$

- L^∞ Stability

$$\exists L > 0, / \max_i |u_i^{(k)}| \leq L, \forall k.$$

These notions of stability will be used also in the nonlinear case, especially for Allen-Cahn's equation. Since there will be no ambiguity, to simplify the notations, we noted in the same way by u the solution of the PDE (6) as well as the time depending solution of the ODE (9) and generally any vector of $I\!R^n$.

Let us first recall a simple but useful result, [8]. We now define the following hypothesis $\mathcal{H}$ that will be used from now on:

Hypothesis $\mathcal{H}$:

i Let A and B be two $n \times n$ Symmetric Semi-Positive Definite matrices (SSPD) with $Ker(A) = Ker(B) = W$

ii. Assume that there exist two strictly positive constants α and β such that

$$\alpha < Bu, u > \leq < Au, u > \leq \beta < Bu, u >, \ \forall u \in I\!R^n. \tag{11}$$

Remark 2.1 *Condition ii. is obviously satisfied for every $u \in W$ and can be alternatively expressed as*

$$\alpha < Bu, u > \leq < Au, u > \leq \beta < Bu, u >, \ \forall u \in W^T.$$

The coefficients α and β can depend on the dimension n. Also both A and B are SDP on W^T.

The simplest stabilized scheme is obtained from Backward Euler's as

$$\frac{u^{(k+1)} - u^{(k)}}{\Delta t} + \tau B(u^{(k+1)} - u^{(k)}) + Au^{(k)} = 0, \tag{12}$$

where $\tau \geq 0$; Forward Euler is recovered for $\tau = 0$ while Backward Euler's is obtained for $\tau = 1$ and $B = A$. We have the stability conditions

Proposition 2.2 *Assume that A and B are two symmetric semi-positive definite matrices and that hypothesis (11) holds. We set $W = Ker(A) = Ker(B)$. Then, we have the following stability conditions:*

- *If $\tau \geq \dfrac{\beta}{2}$, the scheme (12) is unconditionally stable (i.e. stable $\forall\ \Delta t > 0$),*
- *If $\tau < \dfrac{\beta}{2}$, then the scheme is stable for $0 < \Delta t < \dfrac{2}{\left(1 - \frac{2\tau}{\beta}\right)\rho(A)}$.*

Moreover $u^{(k+1)} - u^{(k)} \in W^{\perp}, \forall k \geq 0$.

Proof. The last assertion is obtained directly by using the symmetry of A and B and taking the scalar product with any element of W. Using this property, the rest of the proof is then similar to the one given in [8] when $W = \{0\}$. ■
In [8] was considered Homogeneous Dirichlet Boundary conditions ; the double inequality

$$\alpha < Bu, u > \leq < Au, u > \leq \beta < Bu, u >, \ \forall u \in W^{\perp}$$

in hypothesis (11) allows to consider also periodic or homogeneous Neumann Boundary conditions which are of interest for Phase Fields models, in that case $W = \{(1, 1, \cdots, 1)^T\}$. We will note in the sequel of the paper $\mathbf{1} = (1, 1, \cdots, 1)$; $\mathbf{1}$ is a line vector while $\mathbf{1}^T$ is a column one.

Of course, instead of Euler's method, we can consider second order schemes such Crank Nicolson's and apply the same stabilization procedure:

Proposition 2.3 *Consider the Stabilized Crank Nicolson Scheme*

$$u^{(k+1)} - u^{(k)} + \tau \frac{\Delta t}{2} B(u^{(k+1)} - u^{(k)}) + \Delta t A u^{(k)} = 0$$

Assume that A and B are two symmetric semi-positive definite matrices and that hypothesis (11) holds. We set $W = Ker(A) = Ker(B)$.

- *If $\tau \geq \beta$, the scheme (13) is unconditionally stable (i.e. stable $\forall\ \Delta t > 0$)*
- *If $\tau < \beta$, then the scheme is stable for $0 < \Delta t < \dfrac{2}{\left(1 - \frac{\tau}{\beta}\right)\rho(A)}$.*

Moreover $u^{(k+1)} - u^{(k)} \in W^{\perp}, \forall k \geq 0$.

Proof. It suffices to replace τ by $\frac{\tau}{2}$ in Proposition (2.2). ■

Remark 2.4 *Similar result can be derived for stabilized Gear's scheme:*

$$\frac{1}{2\Delta t}(3u^{(k+1)} - 4u^{(k)} + u^{(k-1)}) + \tau B(u^{(k+1)} - u^{(k)}) + Au^{(k)} = 0.$$

2.2 Discrete Maximum Principle

Another important stability property, crucial in a number of applications, is the L^{∞} stability guaranteed by a maximum principle. We have the

Proposition 2.5 *Assume that $f \geq 0$ and $u^{(0)} \geq 0$. Assume in addition that $Id + \Delta tB$ is a M-matrix for all $\Delta t > 0$. Set $D = \tau B - A$ and $I = \{i \in \{1, \cdots, n\}/D_{ii} < 0\}$. If*

$$D_{i,j} \geq 0, \forall i, j = 1, \cdots, n, i \neq j \text{ and } 0 < \Delta t < \frac{1}{\max_{i \in I} \mid D_{ii} \mid},\ i \in I,$$

then $u^{(k)} \geq 0, \forall k$.

Proof. Let k be fixed and assume that $u^{(k)} \geq 0$. We have

$$(Id + \tau\Delta tB)u^{(k+1)} = (Id + \Delta t(\tau B - A))u^{(k)} + \Delta tf.$$

The matrix $Id + \tau\Delta tB$ is a M-matrix since B is also one, as a direct consequence and a sufficient condition to have $u^{(k+1)} \geq 0$ is $(Id + \Delta t(\tau B - A))u^{(k)} \geq 0$, this is guaranteed when the matrix $R = Id + \Delta t(\tau B - A) = Id + \Delta tD$ has all positive entries, say

$$\begin{cases} 1 + \Delta t(\tau B_{ii} - A_{ii}) \geq 0 & i = 1, \cdots, n, \\ \\ \tau B_{ij} - A_{ij} \geq 0 & i = 1, \cdots, n\, i \neq j. \end{cases}$$

Hence the result by a simple induction. ■

It is usual that the discrete Maximum principle is satisfied for small values of Δt; we recover particularly the conditions that must be satisfied for the Crank-Nicolson scheme taking $\tau = \frac{1}{2}$ and $A = B$, see [29].

2.3 ADI Stabilized Scheme

A important issue for a fast simulation of parabolic equations is the use of splitting methods. We give here stabilized versions of classical ADI schemes. Consider the linear differential system

$$\frac{dU}{dt} + AU = 0,$$

with $A = A_1 + A_2$. Let B_1 and B_2 be pre-conditioners of A_1 and A_2 respectively and $\tau_1,\ \tau_2$ two positive real numbers. All the matrices are supposed to be symmetric positive definite. We introduce the stabilized ADI-schemes

$$\frac{u^{(k+1/2)}-u^{(k)}}{\Delta t}+\tau_1 B_1(u^{(k+1/2)}-u^{(k)})=-A_1u^{(k)}, \tag{13}$$

$$\frac{u^{(k+1)}-u^{(k+1/2)}}{\Delta t}+\tau_2 B_2(u^{(k+1)}-u^{(k+1/2)})=-A_2u^{(k+1/2)}, \tag{14}$$

and the Strang's Splitting

$$\frac{u^{(k+1/3)}-u^{(k)}}{\Delta t/2}+\tau_1 B_1(u^{(k+1/3)}-u^{(k)})=-A_1u^{(k)}, \tag{15}$$

$$\frac{u^{(k+2/3)}-u^{(k+1/3)}}{\Delta t}+\tau_2 B_2(u^{(k+2/3)}-u^{(k+1/3)})=-A_2u^{(k+1/3)}, \tag{16}$$

$$\frac{u^{(k+1)}-u^{(k+2/3)}}{\Delta t/2}+\tau_1 B_1(u^{(k+1)}-u^{(k+2/3)})=-A_1u^{(k+2/3)}. \tag{17}$$

Consider now the general decompositions $A=\sum_{i=1}^{m}A_i$ and $B=\sum_{i=1}^{m}B_i$. We can associate the following RSS-splitting scheme:

$$\frac{u^{(k+i/m)}-u^{(k+(i-1)/m)}}{\Delta t}+\tau_i B_i(u^{(k+i/m)}-u^{(k+(i-1)/m)})=-A_iu^{(k+(i-1)/m)}, i=1,\cdots,m. \tag{18}$$

As a direct consequence of proposition 2.2, we can prove the following result:

Proposition 2.6 *We assume that hypothesis (11) applied to each pair (A_i,B_i) hold and that $W_i = Ker(A_i)=ker(B_i)=W=Ker(A)=Ker(B), i=1,\cdots,m$. Then, the scheme (18) is stable under the following conditions:*

- *If $\tau_i \geq \frac{\beta_i}{2}$,$i=1,\cdots,m$ the scheme (14) is unconditionally stable (i.e. stable $\forall\ \Delta t>0$),*
- *If $\tau_i < \frac{\beta_i}{2}$, $i=1,\cdots,m$, then the scheme is stable for*

$$0<\Delta t<\min_{1\leq i\leq m}\left(\frac{2}{\left(1-\frac{2\tau_i}{\beta_i}\right)\rho(A_i)}\right).$$

Morevover $u^{(k+1)}-u^{(k)}\in W^{\perp},\ \forall k\geq 0$.

Proof. The last assertion is obtained directly by using the symmetry of A_i and B_i and taking the scalar product with any element of W. The rest of the proof is obtained applying proposition 2.2 to each system. ■

2.4 Discretization in space

Before presenting the stabilized schemes for phase fields models, we give hereafter some numerical illustrations on linear problems when discretized in space by finite differences compact schemes, focusing on Neumann boundary conditions. We propose as in [8] to use a (lower) second order discretization matrix for preconditioning the underlining matrices. We first consider the Elliptic Neumann problem then the Heat equation.

2.4.1 Finite difference Preconditioning for compact schemes and the Neumann problem

The 2D and 3D reaction-diffusion problems we will simulate (Allen-Cahn's or Cahn-Hilliard's equations) are completed with Neumann Boundary Conditions; IMEX schemes (IMplicit for the linear terms and EXpicit for the nonlinear ones) need to solve the basic linear problem :

$$\alpha u - \Delta u = f \quad \text{in } \Omega =]0,1[^{2,3}, \tag{19}$$

$$\frac{\partial u}{\partial n} = 0 \qquad \text{on } \partial\Omega, \tag{20}$$

when discretized by second order (RSS) or fourth order compact schemes. If N is the number of discretization points in each direction of the domain Ω, the stiffness matrices are then of respective sizes $N^2 \times N^2$ (2D problem, $n = N^2$) and $N^3 \times N^3$ (3D problem, $n = N^3$). The preconditioning systems can be solved using the cosine DFT.

In two words, the finite differences compact schemes are nonlocal schemes (they have an implicit part), and they allow to reach an accuracy comparable to the spectral one; we refer to the classical book of Collatz [13] and to the seminal paper of Lele [25].

We recall briefly the structure of the compact schemes and resctrict ourselves to the one dimensional case for the sake of simplicity: let $U = (U_1, \cdots, U_N)^T$ denotes a vector whose components are the approximations of a regular function u at (regularly spaced) grid points $x_i = ih$, $i = 1, \cdots, N$. We compute approximations of $V_i = \mathcal{L}(u)(x_i)$ as solution of a system

$$P.V = QU,$$

so the approximation matrix is formally $B = P^{-1}Q$.

There are several ways to build the compact difference scheme associated to a differential operator, especially when non-periodic boundary conditions are present. To obtain a high accuracy at the boundary points while preserving the implicit part of the scheme, an extrapolation scheme is used, see [25] and [8] for the second derivative associated to Neumann Boundary conditions with a fourth order of accuracy: Now applying the same approach, we can consider fourth order compact schemes for the second derivative with associated homogeneous Neumann Boundary conditions

$$P = \begin{pmatrix} 1 & \frac{1}{10} & & & \\ \frac{1}{10} & 1 & \frac{1}{10} & & \\ & \ddots & \ddots & \ddots & \\ & & \frac{1}{10} & 1 & \frac{1}{10} \\ & & & \frac{1}{10} & 1 \end{pmatrix},$$

and

$$Q = \frac{1}{h^2}\begin{pmatrix} a_1 & a_2 & a_3 & a_4 & a_5 & & \\ -\frac{6}{5} & \frac{12}{5} & -\frac{6}{5} & & & & \\ & -\frac{6}{5} & \frac{12}{5} & -\frac{6}{5} & & & \\ & & \ddots & \ddots & \ddots & & \\ & & & -\frac{6}{5} & \frac{12}{5} & -\frac{6}{5} & \\ & & & & -\frac{6}{5} & \frac{12}{5} & -\frac{6}{5} \\ & & a_{N-4} & a_{N-3} & a_{N-2} & a_{N-1} & a_N \end{pmatrix},$$

with

$$\begin{cases} a_1 = a_N = \frac{2681}{480}, \\ a_2 = a_{N-1} = -\frac{32}{3}, \\ a_3 = a_{N-2} = \frac{113}{40}, \\ a_4 = a_{N-3} = -\frac{13}{15}, \\ a_5 = a_{N-4} = \frac{59}{480}. \end{cases}$$

However this presents a drawback: the conservation of the mean value for the discrete heat resolvant is not formally satisfied and instabilities can occur when considering problems in which the mass must be conserved as for the Heat equation (see hereafter) or the Pattern dynamics for Cahn-Hilliard (but this is not the case for inpainting or the segmentation) as shown in Section 4: in these situations the mean value conservation must be forced using a projection step; a modified RSS scheme is then proposed, see hereafter.

The second approach to derive boundary formula is to leave unchanged the explicit part. The following scheme (labelled CS2) is second order accurate at the boundary and fourth order accurate at the interior points:

$$P_{CS2} = \begin{pmatrix} \frac{2}{5} & \frac{1}{5} & & & \\ \frac{1}{10} & 1 & \frac{1}{10} & & \\ & \ddots & \ddots & \ddots & \\ & & \frac{1}{10} & 1 & \frac{1}{10} \\ & & & \frac{1}{5} & \frac{2}{5} \end{pmatrix} \text{ and } Q_{CS2} = \frac{1}{h^2} \begin{pmatrix} -\frac{6}{5} & \frac{6}{5} & & & & & \\ -\frac{6}{5} & \frac{12}{5} & -\frac{6}{5} & & & & \\ & -\frac{6}{5} & \frac{12}{5} & -\frac{6}{5} & & & \\ & & \ddots & \ddots & \ddots & & \\ & & & -\frac{6}{5} & \frac{12}{5} & -\frac{6}{5} & \\ & & & & -\frac{6}{5} & \frac{12}{5} & -\frac{6}{5} \\ & & & & & \frac{6}{5} & -\frac{6}{5} \end{pmatrix}.$$

We represent in Figure 1 (left) the comparison of the spectrum for each of the discretization schemes (second order, Lele's and CS2). We observe the better approximation of the compact schemes to the exact eigenvalues of the operator; particularly the eigenvalues of CS2 and Lele's schemes are very close expect for the last two ones. The lower eigenvalue of CS2 matrix is 0 while the one of Lele's matrix is $-4.5418e-11$. In Figure 1 (right) we displayed the L^∞ error for each discretization scheme when considering the function $u(x) = \cos(x(1-x))$, for different values of the step-size h. We observe a good accordance to the order of accuracy looking to the slopes: 2.0116 (second order scheme and CS2) and 3.8480 for Lele's compact scheme.

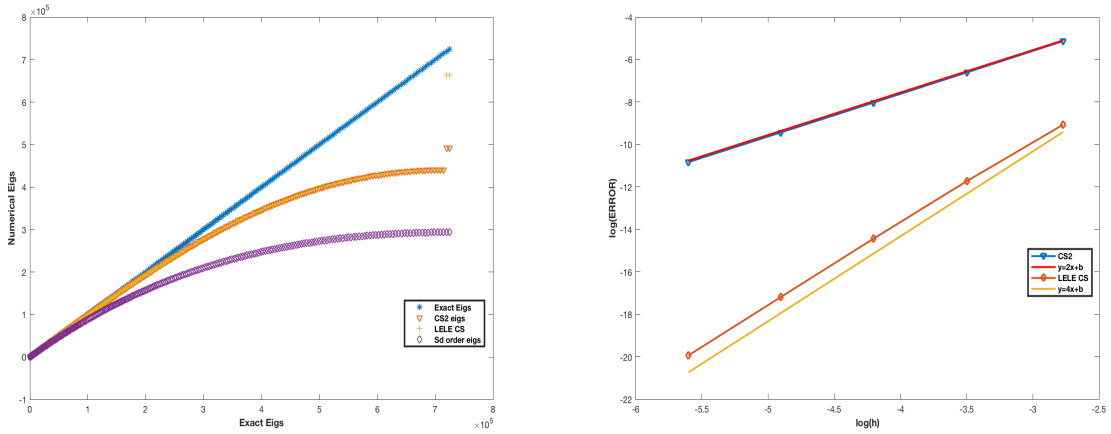

Figure 1: Spectrum of the laplacian matrix discretized with second order and fourth order compact schemes (Lele's and CS2) compared to the exact spectrum of the operator (left); L^∞ error to the function $u(x) = \cos(x(1-x))$ when varying the step-size h, for the 3 schemes - comparison with lines of slope 2 and 4.

The compact schemes of the second order derivative in space dimension 2 and 3, are simply obtained by using the previous schemes and to expand them tensorially.

2.4.2 Heat Equation

Consider the Heat equation:

$$\frac{\partial u}{\partial t} - \Delta u = f, x \in \Omega, t > 0, \tag{21}$$

$$\frac{\partial u}{\partial n} = 0 \quad x \in \partial\Omega, \tag{22}$$

$$u(x,0) = u_0(x) \quad x \in \Omega. \tag{23}$$

When $\int_\Omega f dx = 0$, the solution $u(x,t)$ satisfies $\int_\Omega u(x,t)dx = \int_\Omega u(x,0)dx,\ \forall t > 0$. This important property is fulfilled at the discrete level when the stiffness matrix A enjoys of the property $I_n(Av) = 0$, for all $v \in I\!R^n$, where I_n is a given proper numerical quadrature; for example, when considering the classical second order finite differences laplacian matrix and $I_n(v) = \mathbf{1}^T v/n = Kv$ with $\{\mathbf{1}^T\} = Ker(A)$, the condition on A writes as

$$I_n(Av) =< Av, \mathbf{1}^T/n >= \mathbf{1}Av/n = \frac{1}{n}\sum_{i=1}^{n}\sum_{j=1}^{n} A_{i,j}v_j = 0, \forall v \in I\!R^n,$$

say

$$\sum_{i=1}^{n} A_{i,j} = 0,\ \forall j = 1, \cdots, n.$$

In this case, the Backward Euler's Scheme (1), which is our reference scheme to make comparisons of numerical results,

$$(Id + \Delta t A)u^{(k+1)} = u^{(k)} + \Delta t f^{(k)},$$

allows to reproduce the property at each iteration. Let A_L (resp. A_{CS2}) be the matrix produced by Lele's (resp. by CS2) compact schemes and B be the matrix corresponding to the classical 3 points schemes. We observe that $Ker(B) = Ker(A_{CS2}) = \{\mathbf{1}^T\}$ while $Ker(A_L) \neq \{\mathbf{1}^T\}$ even if $\|A_L\mathbf{1}^T\| \simeq 1.e-11$. Both compact schemes matrices are not symmetric. However their anti-symmetric part is small as compared to the symmetric one, and this has no incidence in practice when considering Dirichlet Boundary Conditions, se also [8]. When the boundary conditions are periodic or homogeneous Neumann the conservation of the mean value is crucial since the accumulation of errors can deteriorate the solution. The null-mean property is important to recover at the discrete level since we will consider splitting schemes in which the linear part consists in solving a time step of a heat equation. For these reasons, and for a sake of simplicity, we propose to impose the mean null property. This can be done by introducing a Lagrange multiplier or by using a splitting scheme with a projection step on the null-mean space, and give rise to modified RSS schemes. We first briefly describe these two procedures for the general case.

2.4.3 Classical scheme

The Backward Euler scheme can be classically interpreted in terms of minimization problem as

$$u^{(k+1)} = arg \min_{u \in I\!R^N} \frac{1}{2}\|F - Mu\|^2,$$

where $F = u^{(k)} + \Delta t f^{(k)}$ and $M = Id + \Delta t A$; $u^{(k+1)}$ satisfies $M^T M u^{(k+1)} = M^T F$ or $Mu^{(k+1)} = F$ since M is invertible. We can impose the null-mean condition in two ways:

Lagrangian approach

First, defining $u^{(k+1)}$ as

$$u^{(k+1)} = arg \min_{u \in I\!R^N I_n(u)=0} \frac{1}{2}\|F - Mu\|^2 = arg \min_{u \in I\!R^N I_n(u)=0} J(u)$$

We look $u^{(k+1)}$ as a critical point of the Lagrangian

$$\mathcal{L}(u,\lambda) = J(u) + \lambda I_n(u) = J(u) + \lambda < \frac{1}{n}\mathbf{1}^T, u > .$$

The optimality relations write as:

$$(Id + \Delta A)^T \Big((Id + \Delta A)u^{(k+1)} - F \Big) + \lambda \frac{1}{n}\mathbf{1}^T = 0, \quad \frac{1}{n}\mathbf{1}u^{(k+1)} = 0.$$

We find formally, after setting $g = M^{-T}\frac{1}{n}\mathbf{1}^T$,

$$\lambda = \frac{< g, F >}{< g, g >}, \tag{24}$$

$$u^{(k+1)} = M^{-1}(F - \lambda g) \tag{25}$$

Projection approach
The second approach consists in centering the solution at each time step, say

$$u^{(k+1)} = M^{-1}F - \frac{< \mathbf{1}^T, M^{-1}F >}{< \mathbf{1}^T, \mathbf{1}^T >}\mathbf{1}^T. \tag{26}$$

When A is symmetric, we define $u^{(k+1)}$ as $arg \min_{u \in I\!R^N, <\mathbf{1}, u>=0} \frac{1}{2} < Mu, u > - < F, u >$ and we derive similar formulae.

2.4.4 RSS modified schemes

We now adapt the previous procedures in the context of the RSS schemes considering the same two approaches.

Lagrangian approach
The matrix here B is assumed to be Symmetric Semi-Definite Positive. We can define $\delta^{(k+1)} = u^{(k+1)} - u^{(k)}$ as minimizing

$$J(\delta) = \frac{1}{2} < M\delta, \delta > + \Delta t < -Au^{(k)}, \delta >,$$

where M is the SPD matrix $Id + \tau \Delta t B$. Hence, to impose the condition $I_n(\delta) = 0$, or equivalently $\delta \perp W = Ker(B)$, we consider rather, e.g., the Lagrangian

$$\mathcal{L}(\delta,\lambda) = J(\delta) + \lambda I_n(\delta) = J(\delta) + \lambda < \frac{1}{n}\mathbf{1}^T, \delta > .$$

The solution of $\inf_{\delta, I_n(\delta)=0} J(\delta)$ is then classically given by the system

$$M\delta + \lambda \frac{1}{n}\mathbf{1}^T = -\Delta t A u^{(k)}, \ \frac{1}{n} < \mathbf{1}^T, \delta >= 0.$$

We find, formally, letting $f = -\Delta t A u^{(k)}$ and $g = \frac{1}{n}M^{-1}\mathbf{1}^T$,

$$\lambda = \frac{< g, f >}{< \frac{1}{n}\mathbf{1}^T, g >} \tag{27}$$

$$\delta = M^{(-1)}f - \lambda g, \tag{28}$$

$$u^{(k+1)} = u^{(k)} + \delta. \tag{29}$$

Projection approach
The second approach consists in a splitting based on a projection step:

$$\delta^{(k+1)} + \tau \Delta t B \delta^{(k+1)} = -\Delta t A u^{(k)}, \tag{30}$$

$$\delta^{(k+1)} := \delta^{(k+1)} - \frac{< \mathbf{1}^T, \delta^{(k+1)} >}{n} \mathbf{1}^T, \tag{31}$$

$$u^{(k+1)} = u^{(k)} + \delta^{(k+1)}. \tag{32}$$

This last method is slightly simple than the previous (Lagrangian) one.

We give hereafter numerical illustration in which we compare the simple RSS and the modified RSS scheme with splitting in 2D and in 3D; both the Lagrangian and the projection schemes give similar results. We simulate the exact solution

$$u(x, y, t) = \cos(2\pi x) \cos(4\pi y) \exp[\sin(t)] \tag{33}$$

and represent in Figures 2 (for $N = 32$) and 3 (for $N = 64$), the time evolution of the mean value and of the error computed in L^∞ norm. We observe that imposing the condition $< \mathbf{1}^T, u^{(k)} >= 0$ allows the stabilized RSS (30)-(32) and the Stabilized Reference Scheme (26) to obtain a normal level of accuracy in time while the error are strongly cumulated when this condition is not satisfied, then when Reference scheme (1) and Standard RSS scheme (12) are applied; the curve are very closed in this last case. Similar results are found when considering CS2 compact schemes for the spatial discretization, see Figure 4. A CPU time reduction si obtained with RSS schemes since the matrix to invert at each iteration is sparse and fast solvers are available. To illustrate the instabilities that can propagate the fourth order Lele's compact

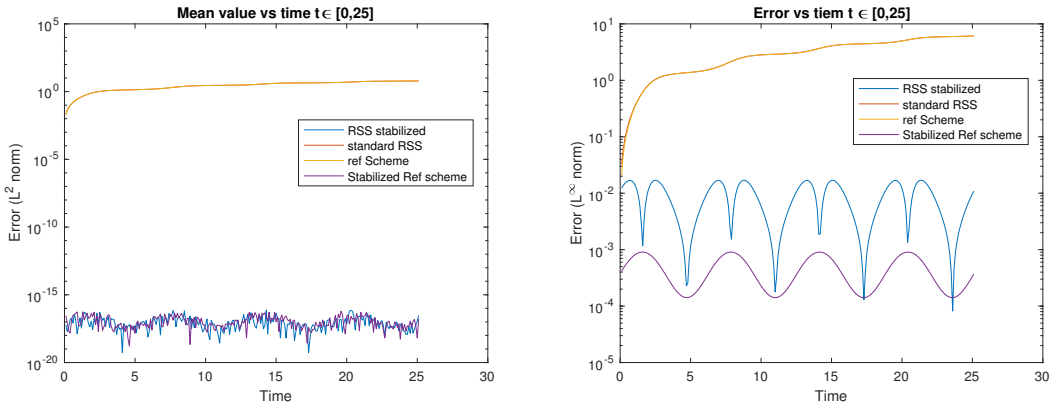

Figure 2: 2D Heat Equation. $N = 32$, $\Delta t = 0.01$, $\tau = 2$. Spatial discretization with Lele's Compact Scheme

scheme, we consider the simulation of the exact solution $u(x, y, t) = \cos(7\pi x) \cos(6\pi y) \exp[\sin(t)]$. In Figure 5, we represent as before the time evolution of the L^∞ error and of the mean value of the solution. While the stabilized reference and RSS schemes using second order and CS2 discretization are stable, the stabilized RSS scheme that uses Lele's CS became numerically unstable. The spectral properties of the discretization matrix of $-\Delta$ reveal to be essential for the stability.

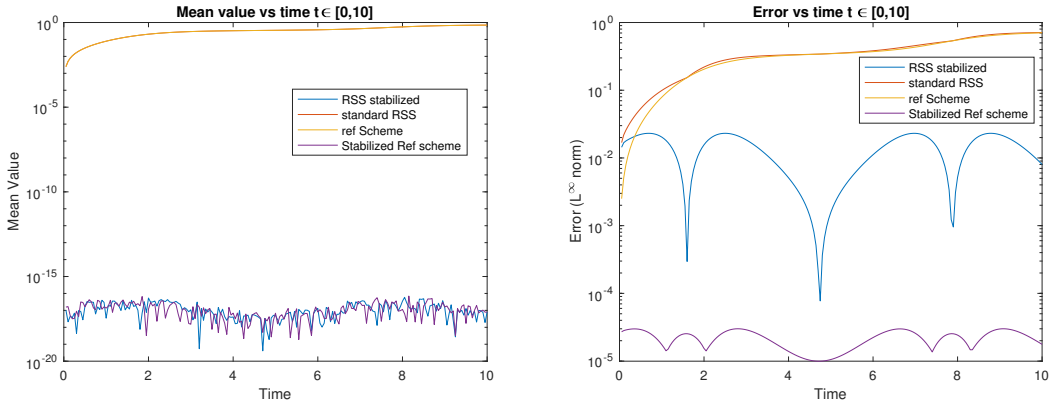

Figure 3: 2D Heat Equation. $N = 64$, $\Delta t = 0.005$, $\tau = 4$. Spatial discretization with Lele's Compact Scheme

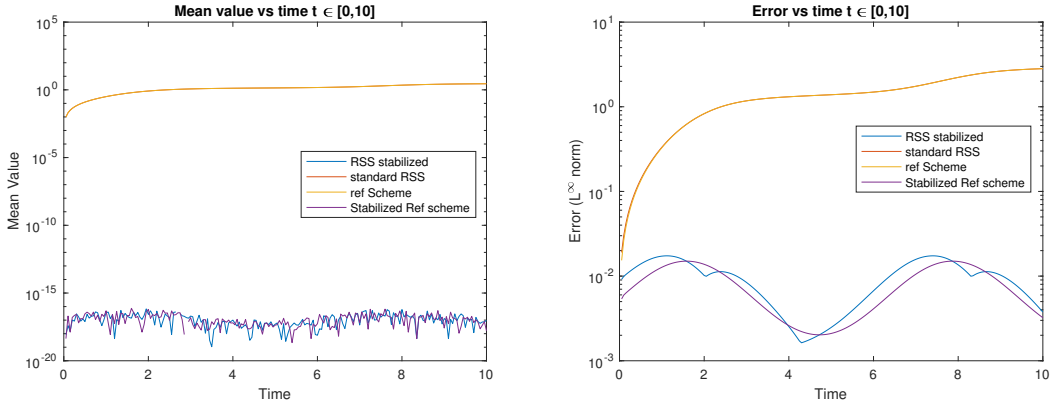

Figure 4: 2D Heat Equation. $N = 32$, $\Delta t = 0.005$, $\tau = 2$. Spatial discretization with CS2 Compact Scheme

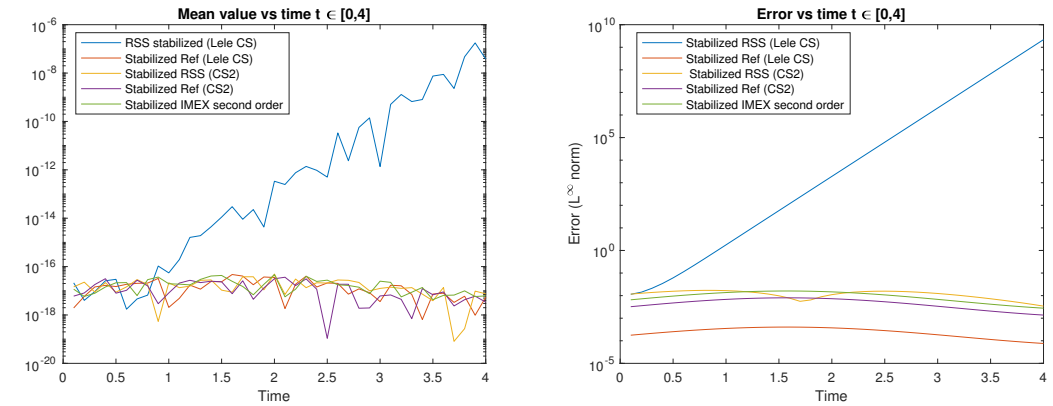

Figure 5: 2D Heat Equation. $N = 64$, $\Delta t = 0.01$, $\tau = 2$. Spatial discretization with CS2 and Lele's Compact Scheme

3 Allen-Cahn's equation

3.1 Phase transition models

3.1.1 Pattern dynamics

Let $\Omega \subset I\!R^n, n = 2, 3$ a regular open bounded set. We here consider the simple Allen-Cahn equation

$$\frac{\partial u}{\partial t} + \mathcal{M}(-\Delta u + \frac{1}{\epsilon^2} f(u)) = 0, \quad x \in \Omega, t > 0, \tag{34}$$

$$\frac{\partial u}{\partial n} = 0 \qquad t > 0, \tag{35}$$

$$u(0, x) = u_0(x), \qquad x \in \Omega. \tag{36}$$

which describes the process of phase separation in iron alloys [2, 3], including order-disorder transitions: $\mathcal{M}$ is the mobility (taken to be 1 for simplicity) and f is the potential that will be taken as the Landau-Lifschitz one $f(u) = u^3 - u$; $F = \int_{-\infty}^{u} f(v)dv$ is the free energy, u is the (non-conserved) order parameter, ϵ is the interface length. The homogenous Neumann boundary conditions imply that there is not a loss of mass outside the domain Ω. It is important to note that here is a competition between the potential term and the diffusion term: regularization in phase transition. Two important properties are satisfied by the solution and must be captured by the numerical scheme (intrinsically or numerically):

- the energy diminishing: Allen-Cahn equation is a gradient flow for the energy

$$E(u) = \frac{1}{2} \int_\Omega \|\nabla u\|^2 dx + \frac{1}{\epsilon^2} F(u)dx,$$

  so $E(u(t)) \leq E(u(t')), \forall t \geq t'$,

- the maximum principle: $|u(., t)|_{L^\infty} \leq L, \forall t > 0$.

3.1.2 Image Segmentation

Image Segmentation consists in labelling pixels in digital images in such a way the image becomes easier to analyse, in particular it allows to locate objects and boundaries. There are many different numerical methods to label data such as KNN (K- Nearest Neighbors) algorithms or Orthogonal Neighborhood Preserving Projection (ONPP) that uses statistical and linear numerical algebra tools respectively, see [23]. Allen-Cahn equations was also proposed as a tool in image segmentation in [26] where the following model is considered:

$$\frac{\partial \phi}{\partial t} - \Delta \phi + \frac{F'(\phi)}{\epsilon^2} + \lambda \left((1 + \phi)(f_0 - c_1)^2 - (1 - \phi)(f_0 - c_2)^2 \right), \quad x \in \Omega, \tag{37}$$

$$\frac{\partial \phi}{\partial n} = 0, \qquad \partial\Omega. \tag{38}$$

If C is the segmenting curve, then the phase ϕ corresponds to the situations

$$\phi(x) = \begin{cases} > 0 & \text{if } x \text{ is inside } C, \\ = 0 & \text{if } x \in C, \\ < 0 & \text{if } x \text{ is outside } C. \end{cases}$$

Here $\epsilon > 0$, $F'(\phi) = \phi(\phi^2 - 1)$, λ is a nonnegative parameter, f_0 is the given image.The terms c_1 and c_2 are the averages of f_0 in the regions $(\phi \geq 0)$ and $(\phi < 0)$, say

$$c_1 = \frac{\int_\Omega f_0(x)(1 + \phi(x))dx}{\int_\Omega (1 + \phi(x))dx} \text{ and } c_2 = \frac{\int_\Omega f_0(x)(1 - \phi(x))dx}{\int_\Omega (1 - \phi(x))dx}.$$

3.2 Energy diminishing schemes

We now turn back to Allen-Cahn pattern dynamics model and after a space discretization we set $E(u) = \frac{1}{2} < Au, u > + \frac{1}{\epsilon^2} < F(u), \mathbf{1}^T >$, for $u \in I\!R^n$, and where F is a primitive of f that we choose such that $F(0) = 0$; $F(u)$ is the vector of $I\!R^n$ which corresponds to a evaluation of F at each components of u. We say that the scheme is energy decreasing if

$$E(u^{(k+1)}) < E(u^{(k)}).$$

The results presented below are extensions of those obtained in [8] and, as in the linear case, the difference is that we can have $W \neq \{0\}$; this situation can have an important influence on the stability results, see Theorem 3.1, hereafter. We first recall some schemes and their stability conditions.

The semi-implicit IMEX Scheme applied to the pattern evolution Allen-Cahn equation:

$$\frac{u^{(k+1)} - u^{(k)}}{\Delta t} + Au^{(k+1)} + \frac{1}{\epsilon^2} f(u^{(k)}) = 0, \tag{39}$$

is energy diminishing under the time step restriction

$$0 < \Delta t < \frac{\epsilon^2 L}{2},$$

where $\mid f' \mid_\infty \leq L$, see [34].

The stabilization of its linear part leads to the scheme

Algorithm 1 : RSS-IMEX for Allen Cahn

1: **for** $k = 0, 1, \cdots$ **do**
2: **Solve** $(Id + \tau \Delta t B)\delta = -\Delta t(Au^{(k)} + \frac{1}{\epsilon^2} f(u^{(k)}))$
3: **Set** $u^{(k+1)} = u^{(k)} + \delta$
4: **end for**

We have the stability result which extends the one given in [8]:

Theorem 3.1 *Assume that hypothesis (11) holds and that f is $\mathcal{C}^1$ and $\mid f' \mid_\infty \leq L$. If $W = \{0\}$ we have then the following stability conditions*

- *If $\tau \geq \frac{\beta}{2}$*
  - *if $\left(\frac{\tau}{\beta} - \frac{1}{2}\right) \lambda_{min}(A) - \frac{L}{2\epsilon^2} \geq 0$ then the scheme is unconditionally stable,*
  - *if $\left(\frac{\tau}{\beta} - \frac{1}{2}\right) \lambda_{min}(A) - \frac{L}{2\epsilon^2} < 0$ then the scheme is stable for*

$$0 < \Delta t < \frac{1}{\frac{L}{2\epsilon^2} - \left(\frac{\tau}{\beta} - \frac{1}{2}\right) \lambda_{min}(A)},$$

- *If $\tau < \frac{\beta}{2}$ then the scheme is stable for*

$$0 < \Delta t < \frac{1}{\frac{L}{2\epsilon^2} - \left(\frac{\tau}{\beta} - \frac{1}{2}\right) \rho(A)}.$$

Here $\lambda_{min}(A)$ denotes the lower strictly positive eigenvalue of A.
If A $W \neq \{0\}$ the stability conditions above apply whenever we assume in addition that $0 < \Delta t < \frac{2\epsilon^2}{L}$.

Proof. For every $k \geq 0$, we decompose every vector u as $u = u_1 + u_2$ with $u_1 \in W^T$ and $u_2 \in W$. We have then

$$\lambda_{min}(A)\|u_1\|_2^2 \leq < Au, u > = < Au_1, u_1 > \leq \rho(A)\|u_1\|_2^2, \text{ and similarly,}$$
$$\lambda_{min}(B)\|u_1\|_2^2 \leq < Bu, u > = < Bu_1, u_1 > \leq \rho(B)\|u_1\|_2^2.$$

Taking the scalar product of the equation $(Id + \tau\Delta t B)\delta = -\Delta t(Au^{(k)} + \frac{1}{\epsilon^2}f(u^{(k)}))$ (line 2 of algorithm) with $\delta = u^{(k+1)} - u^{(k)}$, we find after the usual simplifications (parallelogram identity)

$$\|u^{(k+1)} - u^{(k)}\|^2 + \tau\Delta t < B(u^{(k+1)} - u^{(k)}, u^{(k+1)} - u^{(k)} > -\frac{\Delta t}{2} < A(u^{(k+1)} - u^{(k)}), u^{(k+1)} - u^{(k)} >$$
$$+\frac{\Delta t}{2}\left(< Au^{(k+1)}, u^{(k+1)} > - < Au^{(k)}, u^{(k)} >\right) + \frac{\Delta t}{\epsilon^2} < f(u^{(k)}, u^{(k+1)} - u^{(k)} > = 0.$$

Following [34], we write

$$< F(u^{(k+1)}) - F(u^{(k)}), \mathbf{1} > = < f(u^{(k)}), u^{(k+1)} - u^{(k)} > + \frac{1}{2} < f'(\xi_k)(u^{(k+1)} - u^{(k)}), u^{(k+1)} - u^{(k)} > .$$

Therefore, using hypothesis 11,

$$\|u^{(k+1)} - u^{(k)}\|^2 + \Delta t\left(\frac{\tau}{\beta} - \frac{1}{2}\right) < A(u^{(k+1)} - u^{(k)}), (u^{(k+1)} - u^{(k)}) >$$
$$\leq \frac{L\Delta t}{2\epsilon^2}\|u^{(k+1)} - u^{(k)}\|^2,$$
$$+\frac{\Delta t}{2}\left(< Au^{(k+1)}, u^{(k+1)} > - < Au^{(k)}, u^{(k)} >\right) + \frac{\Delta t}{\epsilon^2} < F(u^{(k+1)}) - F(u^{(k)}), \mathbf{1} > .$$

Finally,

$$(1 - \frac{L\Delta t}{2\epsilon^2})\|u^{(k+1)} - u^{(k)}\|^2 + \Delta t\left(\frac{\tau}{\beta} - \frac{1}{2}\right) < A(u^{(k+1)} - u^{(k)}), u^{(k+1)} - u^{(k)} > + \Delta t\left(E(u^{(k+1)}) - E(u^{(k)})\right) \leq 0,$$

If $W = \{0\}$, then $\lambda_{min}(A)\|u^{(k+1)} - u^{(k)}\|^2 \leq < A(u^{(k+1)} - u^{(k)}), u^{(k+1)} - u^{(k)} > \leq \rho(A)\|u^{(k+1)} - u^{(k)}\|^2$ so

$$(1 - \frac{L\Delta t}{2\epsilon^2} + \Delta t\left(\frac{\tau}{\beta} - \frac{1}{2}\right)\lambda_{min}(A))\|u^{(k+1)} - u^{(k)}\|^2 + \Delta t\left(E(u^{(k+1)}) - E(u^{(k)})\right) \leq 0,$$

if $\frac{\tau}{\beta} - \frac{1}{2} \geq 0$, and

$$(1 - \frac{L\Delta t}{2\epsilon^2} + \Delta t\left(\frac{\tau}{\beta} - \frac{1}{2}\right)\rho(A))\|u^{(k+1)} - u^{(k)}\|^2 + \Delta t\left(E(u^{(k+1)}) - E(u^{(k)})\right) \leq 0,$$

if $\frac{\tau}{\beta} - \frac{1}{2} \leq 0$.

When $W \neq \{0\}$, using the relation $\|u^{(k+1)} - u^{(k)}\|^2 = \|u_1^{(k+1)} - u_1^{(k)}\|^2 + \|u_2^{(k+1)} - u_2^{(k)}\|^2$, we can write

$$(1 - \frac{L\Delta t}{2\epsilon^2})\|u_2^{(k+1)} - u_2^{(k)}\|^2 + (1 - \frac{L\Delta t}{2\epsilon^2})\|u_1^{(k+1)} - u_1^{(k)}\|^2$$
$$+\Delta t\left(\frac{\tau}{\beta} - \frac{1}{2}\right) < A(u_1^{(k+1)} - u_1^{(k)}), u_1^{(k+1)} - u_1^{(k)} > + \Delta t\left(E(u^{(k+1)}) - E(u^{(k)})\right) \leq 0.$$

hence the result. ■

Remark 3.2 *We recover the result given in [8] when $W = \{0\}$ and get enhanced stability as compared to classical IMEX scheme. When $W \neq \{0\}$ the stability conditions are comparable and the advantage of RSS-IMEX is to solve simplified linear part that can be solved fastly.*

A more stable way to overcome the stability restriction is to consider directly Allen-Cahn equation as a gradient system with a natural diminishing energy property. A first unconditionally stable scheme is ([17, 18])

$$\frac{u^{(k+1)}-u^{(k)}}{\Delta t}+Au^{(k+1)}+\frac{1}{\epsilon^2}DF(u^{(k)},u^{(k+1)})=0, \tag{40}$$

where

$$DF(u,v)=\begin{cases}\dfrac{F(u)-F(v)}{u-v} & \text{if } u\neq v,\\ f(u) & \text{if } u=v.\end{cases}$$

In [8] it was introduced the RSS-scheme

$$\frac{u^{(k+1)}-u^{(k)}}{\Delta t}+\tau B(u^{(k+1)}-u^{(k)})+DF(u^{(k+1)},u^{(k)})=-Au^{(k)}, \tag{41}$$

which enjoys of the following stability condition, see [8] for a similar proof.

Proposition 3.3 *Under hypothesis $\mathcal{H}$*

- *if $\tau\geq\frac{\beta}{2}$, the nonlinear RSS scheme (41) is unconditionally stable,*
- *if $\tau<\frac{\beta}{2}$, the nonlinear RSS scheme (41) is stable under condition*

$$0<\Delta t<\frac{\beta}{\rho(A)(\frac{\beta}{2}-\tau)}.$$

An other popular scheme to solve Allen-Cahn is the so-called convex splitting scheme, described in [20, 14], and which is unconditionally stable. We presented in [8] the application of the RSS stabilization to this scheme when W, kernel of A and B, is trivial. Extension to the case $W\neq\{0\}$ can be obtained similarly as previously, so we do not develop this analysis.

3.3 Splitting schemes

We follow [26] who proposed for the so-called double well potential case ($F(u)=\frac{1}{4}(1-u^2)^2$) the following splitting scheme:

$$\frac{u^*-u^{(k)}}{\Delta t}+Au^*=0, \tag{42}$$

$$\frac{u^{(k+1)}-u^*}{\Delta t}=\frac{u^{(k+1)}-(u^{(k+1)})^3}{\epsilon^2}. \tag{43}$$

The last equation can be simplified since it correspond to a one-step approximation by backward Euler's to the differential equation

$$\frac{du}{dt}=\frac{u-u^3}{\epsilon^3}, \tag{44}$$

whose the solution is

$$u(t)=\frac{u(0)}{\sqrt{e^{-2\frac{t}{\epsilon^2}}+u(0)^2(1-e^{-2\frac{t}{\epsilon^2}})}}.$$

Hence the simplified scheme is obtained

$$\frac{u^* - u^{(k)}}{\Delta t} + Au^* = 0, \tag{45}$$

$$u^{(k+1)} = \frac{u^*}{\sqrt{e^{-2\frac{\Delta t}{\epsilon^2}} + (u^*)^2(1 - e^{-2\frac{\Delta t}{\epsilon^2}})}}. \tag{46}$$

We now give here a simple stability result:

Theorem 3.4 *Assume that $Ker(A) = \{\mathbf{1}^T\}$ and that $Id + \Delta tA$ enjoys of the discrete maximum principle. Assume that $|u_i^{(0)}| \leq 1, i = 1, \cdots N$. Then the sequence $u^{(k)}$ defined by (45)- (46) satisfies $|u_i^{(k)}| \leq 1, i = 1, \cdots N$.*

Proof. We proceed by induction. First of all we show that if $|u^{(k)}| \leq 1$ then $|u^{(*)}| \leq 1$. We have

$$(Id + \Delta tA)(u^* - \mathbf{1}) = (u^{(k)} - \mathbf{1}).$$

Hence, by the maximum principle, if $u^{(k)} - \mathbf{1}^T \leq 0$ then $u^{(*)} - \mathbf{1}^T \leq 0$. Replacing $(u^{(k)} - \mathbf{1})$ (resp. $(u^* - \mathbf{1})$) by $(u^{(k)} + \mathbf{1}^T)$ (resp. $(u^* + \mathbf{1}^T)$) we find that $u^{(*)} + \mathbf{1}^T \geq 0$ and conclude that $-1 \leq u^* \leq 1$.
Now, to conclude, it suffices to show that

$$\left|\frac{x}{\sqrt{e^{-2\frac{\Delta t}{\epsilon^2}} + (x)^2(1 - e^{-2\frac{\Delta t}{\epsilon^2}})}}\right| \leq 1 \ \forall x \in [-1, 1], \ \forall \Delta t > 0, \ \forall \epsilon^2 > 0.$$

We set for convenience $\gamma = e^{-2\frac{\Delta t}{\epsilon^2}} \in [0, 1]$. We start from

$$x^2 \leq 1 \iff \gamma x^2 \leq \gamma \iff x^2 \leq (1 - \gamma)x^2 + \gamma \iff \frac{x^2}{(1 - \gamma)x^2 + \gamma} \leq 1.$$

The result is obtained by taking the square-root of this last expression. ■
At this point, we can define a stabilized version of this splitting scheme as

$$\frac{u^* - u^{(k)}}{\Delta t} + \tau B(u^* - u^{(k)}) = -Au^{(k)}, \tag{47}$$

$$u^{(k+1)} = \frac{u^*}{\sqrt{e^{-2\frac{\Delta t}{\epsilon^2}} + (u^*)^2(1 - e^{-2\frac{\Delta t}{\epsilon^2}})}}. \tag{48}$$

To implement RSS-like version of this splitting scheme it then suffices to replace the first step by a RSS-CN scheme as proposed in section 2. We then obtain the RSS-splitting scheme

Algorithm 2 : RSS-splitting for Allen Cahn

1: **for** $k = 0, 1, \cdots$ **do**
2: **Solve** $(Id + \tau\Delta tB)\delta = -\Delta tAu^{(k)}$
3: **Set** $u^{(*)} = u^{(k)} + \delta$
4: **Set** $u^{(k+1)} = \dfrac{u^*}{\sqrt{e^{-2\frac{\Delta t}{\epsilon^2}} + (u^*)^2(1 - e^{-2\frac{\Delta t}{\epsilon^2}})}}$
5: **end for**

As pointed out in the previous section, we do not have generally $A\mathbf{1}^T = 0$ so the mean of solution of the linear step is not conserved. To overcome this problem we project it on the mean-zero vector space and obtain the scheme

Algorithm 3 : RSS-splitting for Allen Cahn with projection

1: **for** $k = 0, 1, \cdots$ **do**
2: **Solve** $(Id + \tau\Delta tB)\delta = -\Delta tAu^{(k)}$
3: **Set** $\delta = \delta - \frac{< \mathbf{1}^T, \delta >}{n}\mathbf{1}^T$
4: **Set** $u^{(*)} = u^{(k)} + \delta$
5: **Set** $u^{(k+1)} = \frac{u^*}{\sqrt{e^{-2\frac{\Delta t}{\epsilon^2}} + (u^*)^2(1 - e^{-2\frac{\Delta t}{\epsilon^2}})}}$
6: **end for**

The proof for the L^∞-stability of the classical θ-scheme with a second order FD matrix is given in ([29]), page 33, but is based on a pointwize analysis.

Theorem 3.5 *We assume that the assumptions of Proposition 2.5 on A and B hold and, in addition, that* $Ker(A) = Ker(B) = \{\mathbf{1}\}$ *and that* $|u_i^{(0)}| \leq 1, i = 1, \cdots N$. *Then the sequence* $u^{(k)}$ *defined by (47)-(48) satisfies* $|u_i^{(k)}| \leq 1, i = 1, \cdots N$

Proof. According to the proof of Theorem 3.4, it suffices to show that if $|u^{(k)}| \leq 1$ then $|u^{(*)}| \leq 1$. This is automatically provided using Proposition 2.5. ■

Remark 3.6 *We gave here sufficient conditions to ensure the stabilized scheme to satisfy a discrete maximum principle. However, this doesn't implies that the scheme is energy decreasing for any* $\Delta t > 0$*: this is observed for small values of* Δt *and moderate values of* τ *; at the contrary large values of* τ *allows to take large time steps but the energy becomes no longer decreasing.*

4 Cahn-Hilliard equation

We here present briefly Cahn-Hilliard equations used for Phase transition and for image inpainting. We introduce new stabilized schemes and establish stability properties.

4.1 The models

4.1.1 Cahn-Hilliard and Patterns dynamics

The Cahn-Hilliard equation describes the process of phase separation, by which the two components of a binary fluid spontaneously separate and form domains pure in each component. It writes as

$$\frac{\partial u}{\partial t} - \Delta(-\Delta u + \frac{1}{\epsilon^2}f(u)) = 0, \tag{49}$$

$$\frac{\partial u}{\partial n} = 0, \tag{50}$$

$$\frac{\partial}{\partial n}\left(\Delta u - \frac{1}{\epsilon^2}f(u)\right) = 0, \tag{51}$$

$$u(0, x) = u_0(x). \tag{52}$$

This equation enjoys of the following properties

- Conservation of the mass: $\bar{u} = \int_\Omega u(x, t)dx = \int_\Omega u_0(x)dx$,
- Decay of the energy in time

$$\frac{\partial E(u)}{\partial t} = -\int_\Omega |\nabla(-\Delta u + \frac{1}{\epsilon^2}f(u))|^2 dx \leq 0.$$

A classical way to study and to simulate Cahn-Hilliard model is to decouple the equation as follows:

$$\frac{\partial u}{\partial t} - \Delta \mu = 0, \qquad \text{in } \Omega, t > 0, \tag{53}$$

$$\mu = -\Delta u + \frac{1}{\epsilon^2} f(u), \qquad \text{in } \Omega, t > 0, \tag{54}$$

$$\frac{\partial u}{\partial n} = 0, \frac{\partial \mu}{\partial n} = 0, \quad \text{on } \partial\Omega, t > 0, \tag{55}$$

$$u(0, x) = u_0(x) \qquad \text{in } \Omega. \tag{56}$$

4.1.2 The inpainting problem

Cahn-Hilliard equations allow here to in paint a tagged picture. Let g be the original image and $D \subset \Omega$ the region of Ω in which the image is deterred. The idea is to add a penalty term that forces the image to remain unchanged in $\Omega \setminus D$ and to reconnect the fields of g inside D, see e.g. [6, 7]. Let $\lambda >> 1$. We have

$$\frac{\partial u}{\partial t} - \Delta(-\epsilon \Delta u + \frac{1}{\epsilon} f(u)) \quad + \lambda \chi_{\Omega \setminus D}(x)(u - g) = 0, \tag{57}$$

$$\underbrace{\text{Cahn-Hilliard equation}} \qquad \underbrace{\text{Fidelity term}} \tag{58}$$

$$\frac{\partial u}{\partial n} = 0 \quad \frac{\partial}{\partial n}\left(\Delta u - \frac{1}{\epsilon^2} f(u)\right) = 0, \tag{59}$$

$$u(0, x) = u_0(x), \qquad x \in \Omega. \tag{60}$$

Here $\chi_{\Omega \setminus D}(x) = \begin{cases} 1 & \text{if } x \in \Omega \setminus D, \\ 0 & \text{else.} \end{cases}$

The presence of the penalization term $\lambda \chi_{\Omega \setminus D}(x)(u - g)$ forces the solution to be close to g in $\Omega \setminus D$ when $\lambda >> 1$; the Cahn-Hilliard flow has as effect to connect the fields inside D. Here ϵ will play the role of the "contrast". A post-processing is possible using the thresholding procedure consisting in replacing the dominant phase by 1 at every point of Ω and the other phases (colors) by 0 to obtain the final inpainting result with a sharp contrast, see also [21, 11] and the references therein.

4.2 The Stabilized Scheme

The semi-implicit scheme

$$\frac{u^{(k+1)} - u^{(k)}}{\Delta t} + A\mu^{(k+1)} = 0, \tag{61}$$

$$\mu^{(k+1)} = \epsilon A u^{(k+1)} + \frac{1}{\epsilon} f(u^{(k)}), \tag{62}$$

suffers from a hard time step restriction, its energy stability is guaranteed for

$$0 < \Delta t < C\epsilon^2,$$

where C is a constant depending on f, see [34]; the stability condition becomes $0 < \Delta t < C\epsilon^4$ when the second equation is $\mu^{(k+1)} = Au^{(k+1)} + \frac{1}{\epsilon^2} f(u^{(k)})$ which do not change the extrema of the energy.

We derive the Stabilized-Scheme from the backward Euler's (61)-(62) by replacing $Az^{(k+1)}$ by $\tau B(z^{(k+1)} - z^{(k)}) + Az^{(k)}$ for $z = u$ or $z = \mu$. We obtain

$$\frac{u^{(k+1)} - u^{(k)}}{\Delta t} + \tau B(\mu^{(k+1)} - \mu^{(k)}) + A\mu^{(k)} = 0, \tag{63}$$

$$\mu^{(k+1)} = \epsilon \tau B(u^{(k+1)} - u^{(k)}) + \epsilon A u^{(k)} + \frac{1}{\epsilon} f(u^{(k)}). \tag{64}$$

At this point we make the following remarks on Steady State of Cahn-Hilliard equation, they are the minimizers of the Energy in the H^{-1} norm. In the considered examples, due to the symmetry properties of the domain and to the conservation of the mass, they are not unique. In such cases, a given steady state $(\mathbf{u}, \mu)$ can be captured by a first scheme while another steady state $(\bar{u}, \bar{\mu}$ can be computed by a different numercical scheme (obtained for instance by varying the time step Δt): this has been observed, e.g., in [9] for nonlinear reaction-diffusion equations exhibiting bifurcations. Here we state that if $(u^{(k)}\mu^{(k)})$ defined by (61)-(62) converges to $(\mathbf{u}, \mu)$ and $(\bar{u}^{(k)}, \bar{\mu}^{(k)})$ defined by (61)-(62) converges to $(\bar{\mathbf{u}}, \bar{\mu})$, then both $(\mathbf{u}, \mu)$ and $(\bar{\mathbf{u}}, \bar{\mu})$ are steady state of the discrete system

$$\begin{aligned} &A\mu = 0, \\ &\mu = \epsilon A u + \tfrac{1}{\epsilon} f(u). \end{aligned}$$

When $(u_0, \mathbf{1}^T) = 0$ and $Ker(A) = Ker(B) = \{\mathbf{1}^T\}$, the steady states have all the mean-zero property. In that way, the stabilization term does There is not guaranty that $(\mathbf{u}, \mu) = (\bar{\mathbf{u}}, \bar{\mu})$ however, we observe numerically that the energy of the two steady states is the same. To go further in this topic, we mention the work of B. Merlet and M. Pierre on the convergence to the equilibrium for gradient flows[28].

We now address a stability analysis.

Theorem 4.1 *Assume that A and B satisfy the hypothesis (11), we note $W = Ker(A) = Ker(B)$. We have the following stability conditions in the linear and in the nonlinear case:*

- *Linear case $f \equiv 0$: If $\tau \geq \beta$, then the scheme (63)-(64) is unconditionally stable.*
- *Nonlinear case: If $\tau \geq max(\beta, \frac{L}{2\epsilon^2 \lambda_{min}(B)} + \frac{\beta}{2})$, then the scheme (63)-(64) is unconditionally stable. Here $\lambda_{min}(B) > 0$ is the smallest strictly positive eigenvalue of B, i.e. $\lambda_{min}(B) = \mathrm{Min}_{x \in W^T, \|x\|=1} < Bx, x >$.*

In addition $u^{(k+1)} - u^{(k)} \in W^{\perp}$, $\forall k \geq 0$, in particular, if $W = \{\mathbf{1}^T\}$, the mean value of $u^{(k)}$ is conserved.

Proof. We first prove directly that $u^{(k+1)} - u^{(k)} \in W^{\perp}, \forall k \geq 0$ by taking the scalar product with any element of $W = Ker(A) = Ker(B)$ in the first system. We begin by considering the linear case ($f \equiv 0$). We take the scalar product of (63) with $\mu^{(k+1)}$ and of (64) with $u^{(k+1)} - u^{(k)}$. After the use of the parallelogram identity and usual simplifications, we obtain, on the one hand

$$\begin{aligned} &< u^{(k+1)} - u^{(k)}, \mu^{(k+1)} > + \frac{\Delta t \tau}{2} \left(< B\mu^{(k+1)}, \mu^{(k+1)} > - < B\mu^{(k)}, \mu^{(k)} > \right. \\ &\left. + < B(\mu^{(k+1)} - \mu^{(k)}), \mu^{(k+1)} - \mu^{(k)} > \right) + \frac{\Delta t}{2} \left(< A\mu^{(k+1)}, \mu^{(k+1)} > + < A\mu^{(k)}, \mu^{(k)} > \right. \\ &\left. - < A(\mu^{(k+1)} - \mu^{(k)}), \mu^{(k+1)} - \mu^{(k)} > \right) = 0, \end{aligned}$$

and on the other hand

$$\begin{aligned} < u^{(k+1)} - u^{(k)}, \mu^{(k+1)} > \; &= \tau\epsilon < B(u^{(k+1)} - u^{(k)}), u^{(k+1)} - u^{(k)} > \\ &+ \frac{1}{2}\epsilon \left(< Au^{(k+1)}, u^{(k+1)} > - < Au^{(k)}, u^{(k)} > \right) \\ &- \frac{1}{2}\epsilon < A(u^{(k+1)} - u^{(k)}), u^{(k+1)} - u^{(k)} > . \end{aligned}$$

Taking the difference of the last two identities, we obtain, after the usual simplifications

$$\begin{aligned} &\epsilon \{ \tau < B(u^{(k+1)} - u^{(k)}), u^{(k+1)} - u^{(k)} > - \frac{1}{2} < A(u^{(k+1)} - u^{(k)}), u^{(k+1)} - u^{(k)} > \} \\ &+ \frac{\Delta t}{2} \{ \tau < B(\mu^{(k+1)} - \mu^{(k)}), \mu^{(k+1)} - \mu^{(k)} > - < A(\mu^{(k+1)} - \mu^{(k)}), \mu^{(k+1)} - \mu^{(k)} > \} \\ &+ R^{k+1} - R^k = 0, \end{aligned}$$

where

$$R^{k+1} = \frac{1}{2}\epsilon < Au^{(k+1)}, u^{(k+1)} > + \frac{\Delta t}{2} < B\mu^{(k+1)}, \mu^{(k+1)} > .$$

The scheme is then stable when $R^{k+1} \leq R^k$. Now using (11), we obtain

$$\epsilon\{\tau < B(u^{(k+1)} - u^{(k)}), u^{(k+1)} - u^{(k)} > -\frac{1}{2} < A(u^{(k+1)} - u^{(k)}), u^{(k+1)} - u^{(k)} >\}$$
$$+\frac{\Delta t}{2}\{\tau < B(\mu^{(k+1)} - \mu^{(k)}), \mu^{(k+1)} - \mu^{(k)} > - < A(\mu^{(k+1)} - \mu^{(k)}), \mu^{(k+1)} - \mu^{(k)} >\}$$
$$\leq \epsilon\{\tau - \frac{\beta}{2}\} < B(\mu^{(k+1)} - \mu^{(k)}), \mu^{(k+1)} - \mu^{(k)} > +\frac{\Delta t}{2}\{\tau - \beta\} < B(\mu^{(k+1)} - \mu^{(k)}), \mu^{(k+1)} - \mu^{(k)} > .$$

Hence the sufficient stability conditions.
Consider now the general case $f \neq 0$. First of all, as in [34], we take the Taylor expansion of the term $\frac{1}{\epsilon}f(u^{(k)}) = \frac{1}{\epsilon} < F(u^{(k+1)}) - F(u^{(k)}), \mathbf{1}^T > +\frac{1}{2\epsilon} < f'(\xi^{(k)})(u^{(k+1)} - u^{(k)}), u^{(k+1)} - u^{(k)} >$. Hence, we deduce from the previous inequality

$$\epsilon\{\tau - \frac{\beta}{2}\} < B(u^{(k+1)} - u^{(k)}), u^{(k+1)} - u^{(k)} > +\frac{\Delta t}{2}\{\tau - \beta\} < B(\mu^{(k+1)} - \mu^{(k)}), \mu^{(k+1)} - \mu^{(k)} >$$
$$+E^{k+1} - E^k \leq \frac{L}{2\epsilon}\|u^{(k+1)} - u^{(k)}\|^2,$$

where $L = \|f'(u)\|_\infty$ and

$$E^{k+1} = \frac{1}{2}\epsilon < Au^{(k+1)}, u^{(k+1)} > +\frac{\Delta t}{2} < B\mu^{(k+1)}, \mu^{(k+1)} > +\frac{1}{\epsilon} < F(u^{(k+1)}) - F(u^{(k)}), \mathbf{1}^T > .$$

At this point, we use the bounds of the Rayleigh quotient of matrix B:

$$\lambda_{min}(B)\|u\|^2 \leq < Bu, u > \leq \lambda_{max}(B)\|u\|^2, \forall u \in W^\perp,$$

so, if $\tau > \beta$, then

$$\left(\lambda_{min}(B)\epsilon(\tau - \frac{\beta}{2}) - \frac{L}{2\epsilon}\right)\|u^{(k+1)} - u^{(k)}\|^2 + \frac{\Delta t}{2}(\tau - \beta) < B(\mu^{(k+1)} - \mu^{(k)}), \mu^{(k+1)} - \mu^{(k)} >$$
$$+E^{k+1} - E^k \leq 0.$$

We find the unconditional stability condition

$$\tau \geq max(\beta, \frac{L}{2\epsilon^2\lambda_{min}(B)} + \frac{\beta}{2}).$$

■
We can now give other stability results for nonlinear RSS schemes. We first consider

$$\frac{u^{(k+1)} - u^{(k)}}{\Delta t} + \tau B(\mu^{(k+1)} - \mu^{(k)}) + A\mu^{(k)} = 0, \tag{65}$$
$$\mu^{(k+1)} = \epsilon\tau B(u^{(k+1)} - u^{(k)}) + \epsilon Au^{(k)} + \frac{1}{\epsilon}DF(u^{(k+1)}, u^{(k)}). \tag{66}$$

where $DF(u^{(k+1)}, u^{(k)})$ is defined in Section 3.2.

Theorem 4.2 *If $\tau > \beta$, then the scheme (65)-(66) is unconditionally stable and $< u^{(k+1)} - u^{(k)}, \mathbf{1}^T >= 0$, $\forall k \geq 0$.*

Proof. We proceed exactly as in Theorem 4.1. We obtain after the usual simplifications

$$\epsilon\{\tau < B(u^{(k+1)} - u^{(k)}), u^{(k+1)} - u^{(k)} > -\frac{1}{2} < A(u^{(k+1)} - u^{(k)}), u^{(k+1)} - u^{(k)} >\}$$
$$+\frac{\Delta t}{2}\{\tau < B(\mu^{(k+1)} - \mu^{(k)}), \mu^{(k+1)} - \mu^{(k)} > - < A(\mu^{(k+1)} - \mu^{(k)}), \mu^{(k+1)} - \mu^{(k)} >\}$$
$$+E^{k+1} - E^k \leq 0.$$

Hence the sufficient stability conditions. ■

Remark 4.3 *The stabilization procedure differs from the one used in [34] which applied her gives rise to the modified scheme:*

$$\frac{u^{(k+1)}-u^{(k)}}{\Delta t}+A\mu^{(k+1)}=0, \tag{67}$$

$$\mu^{(k+1)}=\epsilon Au^{(k+1)}+\frac{S}{\epsilon}(u^{(k+1)}-u^{(k)})+\frac{1}{\epsilon}f(u^{(k)}). \tag{68}$$

The parameter S is then tuned to obtain a more stable scheme, however for large values of $\tau'=\frac{S}{\epsilon}$ it slows down the dynamics, particularly the energy decreases at a lower rate than that of a reference scheme, see also [1, 8] for Allen-Cahn equation.

We now describe the practical solution. We can write

$$\begin{pmatrix} Id & \tau\Delta tB \\ -\epsilon\tau B & Id \end{pmatrix}\begin{pmatrix} u^{(k+1)}-u^{(k)} \\ \mu^{(k+1)} \end{pmatrix}=\begin{pmatrix} -\Delta tA\mu^{(k)} \\ \epsilon Au^{(k)}+\frac{1}{\epsilon}f(u^{(k)}) \end{pmatrix}.$$

The matrix of the system can be factorized as Block LU

$$M=\begin{pmatrix} Id & \tau\Delta tB \\ -\epsilon\tau B & Id \end{pmatrix}=\begin{pmatrix} Id & 0 \\ -\epsilon\tau B & Id \end{pmatrix}\begin{pmatrix} Id & \tau\Delta tB \\ 0 & S \end{pmatrix},$$

where $S=Id+\tau^2\Delta t\epsilon B^2$ is the Schur complement. We have to solve the coupled linear system

$$\begin{cases} X_1+\tau\Delta tBX_2=F1, \\ -\tau\epsilon BX_1+X_2=F_2. \end{cases}$$

Hence

$$(Id+\tau^2\Delta t\epsilon B^2)X_2=F_2+\epsilon\tau BF1.$$

Then,

$$X_1=F_1-\tau\Delta tBX_2.$$

We can resume the implementation of (63)-(64) which gives rise to the RSS-IMEX scheme, reads as:

Algorithm 4 : RSS-IMEX Cahn-Hilliard for Pattern Dynamics

1: **for** $k=0,1,\cdots$ until convergence **do**
2: **Set** $F_1=-\Delta tA\mu^{(k)}$ and $F_2=-\mu^{(k)}+\epsilon Au^{(k)}+\frac{1}{\epsilon}f(u^{(k)})$
3: **Solve** $(Id+\tau^2\Delta t\epsilon B^2)\delta\mu=F_2+\tau\epsilon BF_1$
4: **Set** $\mu^{(k+1)}=\mu^{(k)}+\delta\mu$
5: **Set** $\delta u=F_1-\tau\Delta tB\delta\mu$
6: **Set** $\delta u=\delta u-\frac{<\mathbf{1}^T,\delta u>}{n}\mathbf{1}^T$
7: **Set** $u^{(k+1)}=u^{(k)}+\delta u$
8: **end for**

The nonlinear RSS scheme, say the implementation of (65)-(66) which gives rise to the NLRSS, can be obtained with inner fixed point iterations as following:

Algorithm 5 : NLRSS Cahn-Hilliard for Pattern Dynamics

for $k = 0, 1, \cdots$ **do**
  Set $u^{(k,0)} = u^{(k)}$
  for $m = 0, 1, \cdots$ until convergence **do**
    Set $F_1 = -\Delta t A \mu^{(k)}$
    Set $F_2 = -\mu^{(k)} + \epsilon A u^{(k)} + \frac{1}{\epsilon} DF f(u^{(k,m)}, u^{(k)})$
    Solve $(Id + \tau^2 \Delta t \epsilon B^2)\delta\mu = F_2 + \tau\epsilon B F_1$
    Set $\mu^{(k,m+1)} = \mu^{(k)} + \delta\mu$
    Set $\delta u = F_1 - \tau \Delta t B \delta\mu$
    Set $\delta u = \delta u - \frac{<\mathbf{1}^T, \delta u>}{n} \mathbf{1}^T$
    Set $u^{(k,m+1)} = u^{(k)} + \delta u$
  end for
  Set $\mu^{(k+1)} = \mu^{(k,m+1)}$
  Set $u^{(k+1)} = u^{(k,m+1)}$
end for

When considering the inpainting model, the RSS-IMEX scheme can be written as

$$\frac{u^{(k+1)} - u^{(k)}}{\Delta t} + \tau B(\mu^{(k+1)} - \mu^{(k)}) + A\mu^{(k)} + \lambda_0 D(u^{(k+1)} - g) = 0, \tag{69}$$

$$\mu^{(k+1)} = \epsilon\tau B(u^{(k+1)} - u^{(k)}) + \epsilon A u^{(k)} + \frac{1}{\epsilon} f(u^{(k)}). \tag{70}$$

say in the matricial form

$$\begin{pmatrix} Id + \Delta t \lambda_0 D & \tau \Delta t B \\ -\epsilon\tau B & Id \end{pmatrix} \begin{pmatrix} u^{(k+1)} - u^{(k)} \\ \mu^{(k+1)} - \mu^{(k)} \end{pmatrix} = \begin{pmatrix} \Delta t(\lambda_0 D(g - u^{(k)}) - A\mu^{(k)}) \\ \epsilon A u^{(k)} + \frac{1}{\epsilon} f(u^{(k)}) - \mu^{(k)} \end{pmatrix}.$$

The implementation of the scheme reads as

Algorithm 6 : RSS-IMEX Cahn-Hilliard for inpainting

for $k = 0, 1, \cdots$ until convergence **do**
  Set $F_1 = \Delta t(\lambda_0 D(g - u^{(k)}) - A\mu^{(k)})$
  Set $F_2 = -\mu^{(k)} + \epsilon A u^{(k)} + \frac{1}{\epsilon} f(u^{(k)})$
  Solve $(Id + \Delta t \lambda_0 D + \tau^2 \Delta t \epsilon B^2)\delta u = F_1 - \tau \Delta t B F_2$
  Set $\delta\mu = F_2 + \epsilon\tau B\delta$
  Set $u^{(k+1)} = u^{(k)} + \delta u$
  Set $\mu^{(k+1)} = \mu^{(k)} + \delta\mu$
end for

Remark 4.4 *Stabilization of semi-implicit scheme for Cahn-Hilliard equations have been considered, e.g. in [6, 7, 21] for inpainting problems,*

$$\frac{u^{(k+1)} - u^{(k)}}{\Delta t} + A\mu^{(k+1)} + c_1 A(u^{(k+1)} - u^{(k)}) + c_2(u^{(k+1)} - u^{(k)}) + \lambda_0 D(u^{(k)} - g) = 0, \tag{71}$$

$$\mu^{(k+1)} = \epsilon A u^{(k+1)} + \frac{1}{\epsilon} f(u^{(k)}). \tag{72}$$

Here c_1 and c_2 are positive constants, they play the role of stabilization parameters. Large values of c_1 and c_2 allow to take large time step, however it damages the dynamics. Our approach is here different.

5 Numerical Results

5.1 Implementation

The applications we are interested with are Allen-Cahn and Cahn-Hilliard equations to which homogeneous Neumann boundary conditions are associated. We proceed as in [8] and we first discretize in space the equation with high order finite difference compact schemes as described in section 2.4.1: the matrix A corresponds to the laplacean with Homogenous Neumann BC (HNBC) when using compact schemes while matrix B is the (sparse) second order laplacean matrix with Neumann Homogeneous Boundary conditions.

Also, the mean-zero property of the linear part of Allen-Cahn equations (for splitting schemes) and for Cahn-Hilliard equations is imposed by the projection described in Section 2.4.4.
All the computations have been realized using Matlab ®. For a fast solution of linear systems in the RSS-like schemes, we will use the cosine-FFT to solve the Neumann problems with matrix $Id + \tau\Delta t B$. More precisely the Discrete Cosine Transform (DCT) `dct.m` (resp. `idct.m` for the inverse discrete transform), in space dimension 2 and `mirt_dctn.m` (resp. `mirt_idctn.m`), this last routine is due to Andriy Myronenko, and can be found at
`https://mathworks.com/matlabcentral/profile/authors/1834156-andriy-myronenko`. We refer also the reader to [36] for a review on DCT.

5.2 Allen-Cahn equation

5.2.1 Pattern Dynamics

To point out the fast solution of the RSS schemes as compared to the reference IMEX one and to illustrate the influence of the stabilization on the accuracy of the computed solution, we compare the reference IMEX scheme (39) with RRS- stabilizations RSS-IMEX (Algo. 3.2) and RSS-Splitting (Algo. 3). We will consider 2D then 3D Allen-Cahn equation.

At first, to compare the accuracy of these methods, and point out the influence of the stabilizing parameter τ, we simulate the solution $u(x, y, t) = \cos(2\pi x)\cos(2\pi y)\exp(\sin(t))$ of the 2D forced Allen-Cahn equation, adding a source term defined by $f(x, y, t) = u_t - \Delta u + \frac{1}{\epsilon^2}u(u^2 - 1)$. In Figures **??** and 6, we plotted the time evolution of the L^∞ norm of the error $e_\infty = \|u^n - u(\cdot, \cdot, t^n)\|_\infty$ when taking $\tau = 2$ and $\tau = 100$. We observe that, using CS2 compact schemes, that a moderate value of τ allows the RSS-IMEX scheme to obtain an accuracy comparable to the reference IMEX one; similar behavior is observed when considering Lele's Schemes (Figure 6 on the left). At the contrary, a large value of τ, say $\tau = 100$ deteriorate the precision of the RSS-IMEX scheme (Figure 6 on the right). We observe that RSS-Splitting does not allows to obtain a satisfactory accuracy.

We now focus on the gain computing time obtained when using RSS schemes as compared to the reference IMEX one. We consider the direct simulation (say without a source term) of Allen-Cahn's equation in space dimension 2 and 3. We take $\varepsilon = 0.01$ an we used here CS2 compact schemes for the space discretization and used the 2 dimensional cosine DFT for the solution of the linear systems in the RSS schemes; similar results are obtained using Lele's compact scheme.
In 2D, we chose $u_0(x, y) = \cos(\pi x)\cos(2\pi y)$ and in 3D $u_0(x, y) = \cos(\pi x)\cos(2\pi y)\cos(6z)$.
The 2D results are reported in Table 1 the 3D ones in Table 2, for different values of N, the number of discretization point sin each direction of the domain. The CPU time reduction obtained with RSS-schemes is clearly very important and increases with the number of unknowns and the dimension (N^2 in 2D and N^3 in 3D). We observe in Figure 7 that the IMEX-RSS produces comparable solution to IMEX scheme for moderate values of τ (this is not the case with RSS-Splitting for which we observe that large values of τ of of Δt do not make the energy decreasing in time), see illustrations below.

We report in In Figure 8 the time evolution of the energy for the different schemes.

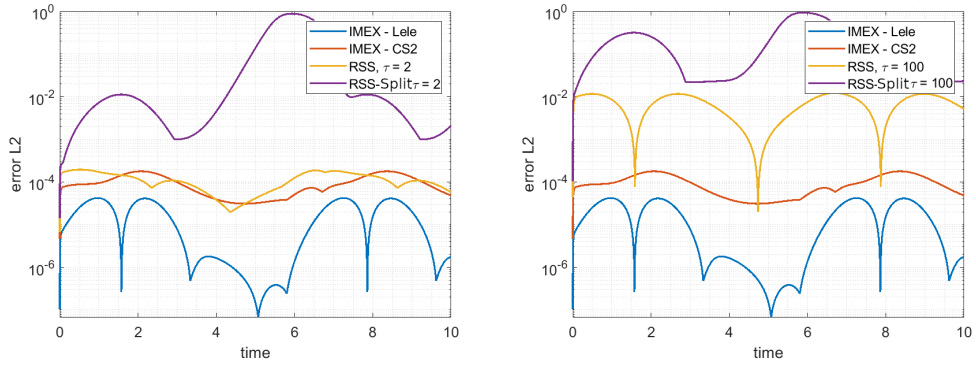

Figure 6: 2D Allen-Cahn equations. Error e_∞ considering the time schemes IMEX, RSS and RSS-Splitting rely on CS2. We add a curve corresponding to IMEX rely on Lele's space discretisation. The exact solution is $u(x,y,t) = \cos(2\pi x)\cos(2\pi y)\exp(\sin(t))$ and $\varepsilon = 0.5$. The numerical parameters are $N = 64$ and $\Delta t = 10^{-4}$.

	IMEX (Algo. (39)	RSS-IMEX (Algo. 3.2)($\tau = 2$)	RSS-Splitting (Algo. 3)($\tau = 2$)
CPU time $N = 16$	2.3809	0.5199	0.61618
CPU time $N = 32$	19.2752	0.72124	0.7424
CPU time $N = 64$	426.7139	3.5574	3.4405
CPU time $N = 128$	too long	21.6112	21.6212

Table 1: 2D Allen-Cahn equation. Final time $t_{\max} = 0.01$, $\Delta t = 0.0001$, $\varepsilon = 0.01$. CPU time in seconds.

	IMEX (Algo. 39)	RSS-IMEX (Algo. 3.2)($\tau = 2$)	RSS-Splitting (Algo. 3)($\tau = 2$)
CPU time $N = 8$	5.1924	0.7246	0.8054
CPU time $N = 16$	313.8788	2.1995	2.0523
CPU time $N = 32$	too long.	19.3381	18.9964
CPU time $N = 64$	too long.	353.88	363.0721

Table 2: 3D Allen-Cahn equation. Final time $t_{\max} = 0.01$, $\Delta t = 0.0001$, $\varepsilon = 0.01$. CPU time in seconds.

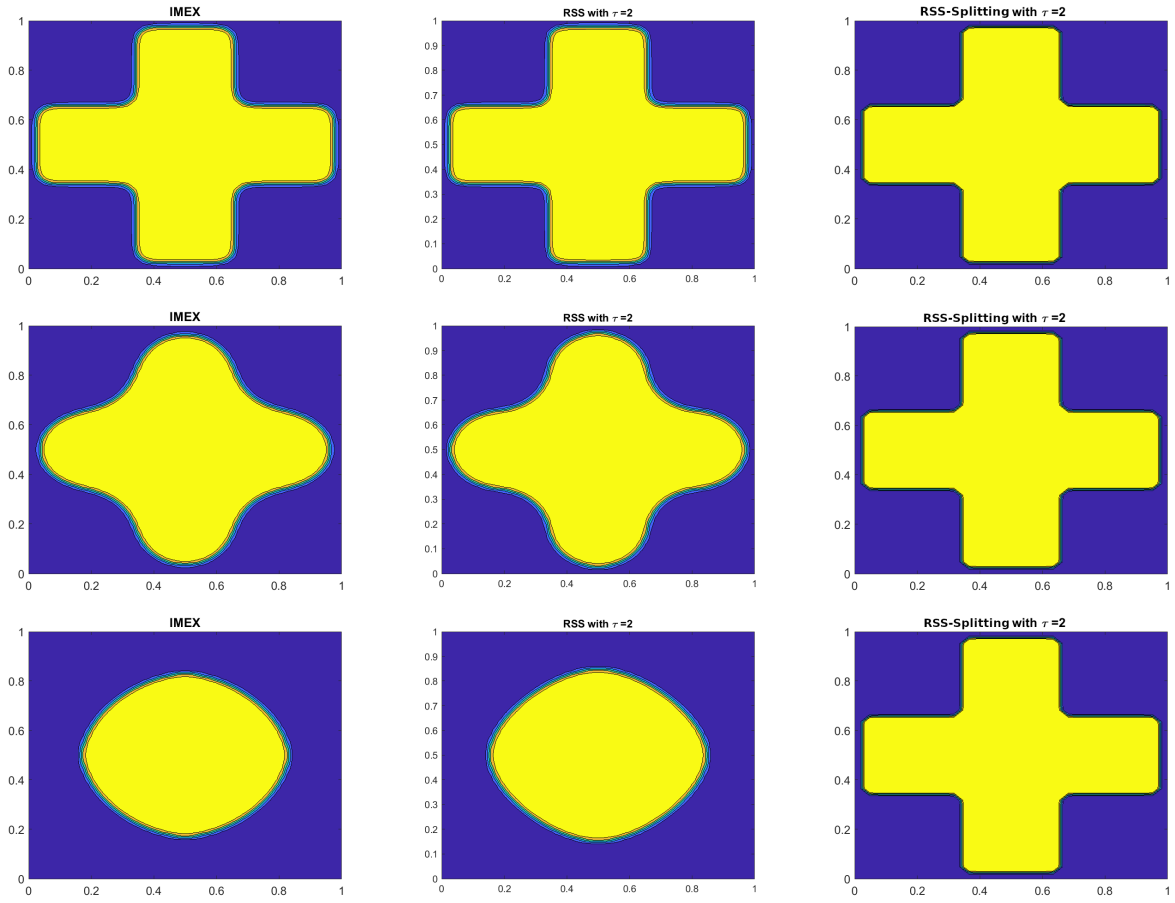

Figure 7: Solution of the 2D Allen-Cahn equation with different time schemes. The initial condition is a given cross. Line by line, the numerical solution are at time $t = 10^{-3}$, $t = 0.01$ and $t = 0.05$. The parameters are $\varepsilon = 10^{-2}$, $N = 64$, $\Delta t = 10^{-4}$ and $\tau = 2$.

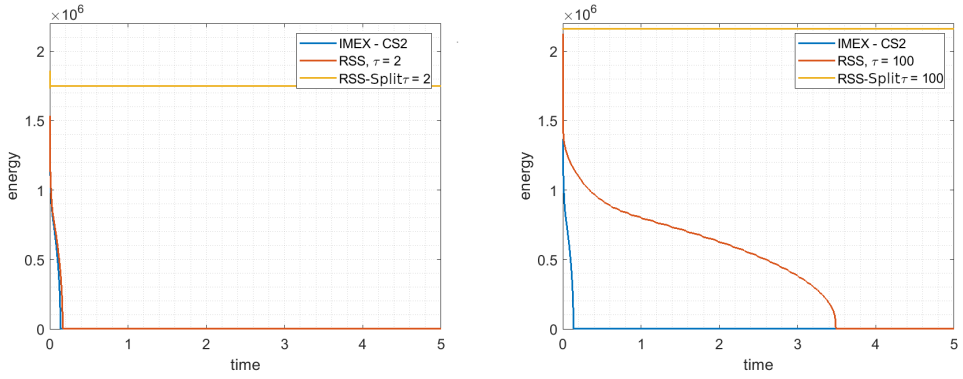

Figure 8: History of the numerical energy for the 2D Allen-Cahn equation with different time schemes. The initial condition is is a given cross. The parameters are $\varepsilon = 10^{-2}$, $N = 64$, $\Delta t = 10^{-4}$ and $\tau = 2$ (left) and $\tau = 100$ (right) .

We now give illustrations on the solution of 3D Allen Cahn equations. We observe in Figure 9 that the numerical solutions converge to one of the constant steady states $\bar{u}_+ = 1$ and $\bar{u}_- = -1$ which are the to global minimizers of the energy: $E(\bar{u}_+) = E(\bar{u}_-) = 0$, more precisely $\bar{u}_+ = 1$ for IMEX and RSS-IMEX and $\bar{u}_- = -1$ for RSS-Splitting. We observe in Figure 10 that this last method does not capture the dynamics of the energy for $\tau = 2$ and $\tau = 100$ while RSS-IMEX give comparable results.

As shown above, the splitting scheme can enjoy of a discrete maximum property, for sufficiently small Δt, however there is no guarantee of a decreasing of the energy if Δt is not small enough. We observe here, for the same numerical and physical data that the RSS-IMEX scheme allows to capture the dynamics while this is not the case with the Splitting RSS.

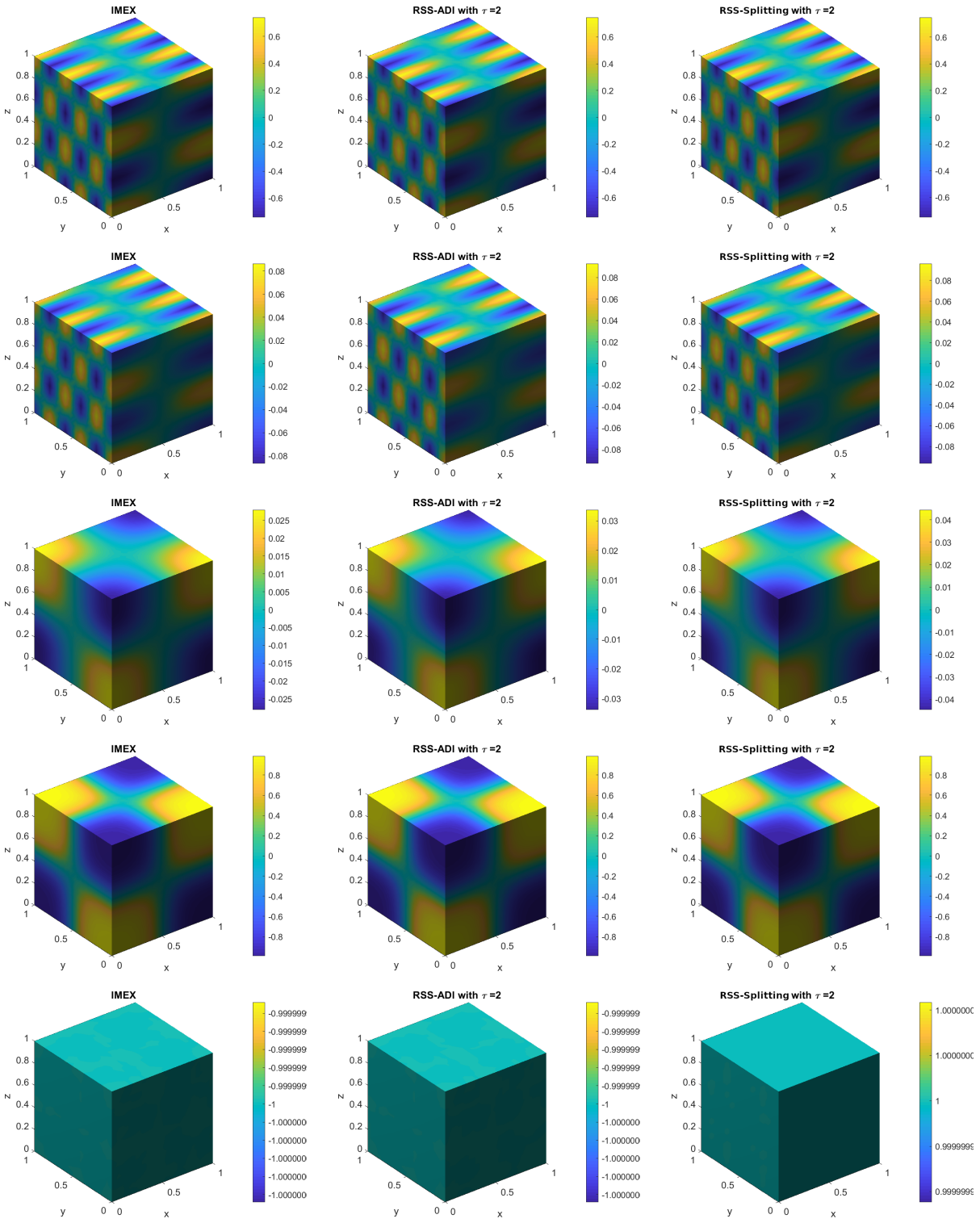

Figure 9: Solution of the 3D Allen-Cahn equation with different time schemes. The initial condition is $u_0(x, y, z) = \cos(\pi x)\cos(5\pi y)\cos(3\pi z)$. Line by line, the numerical solution are at time $t = 10^{-3}$, $t = 10^{-2}$, $t = 0.1$, $t = 0.5$ and $t = 1$. The parameters are $\varepsilon = 0.1$, $N = 16$, $\Delta t = 10^{-4}$ and $\tau = 2$.

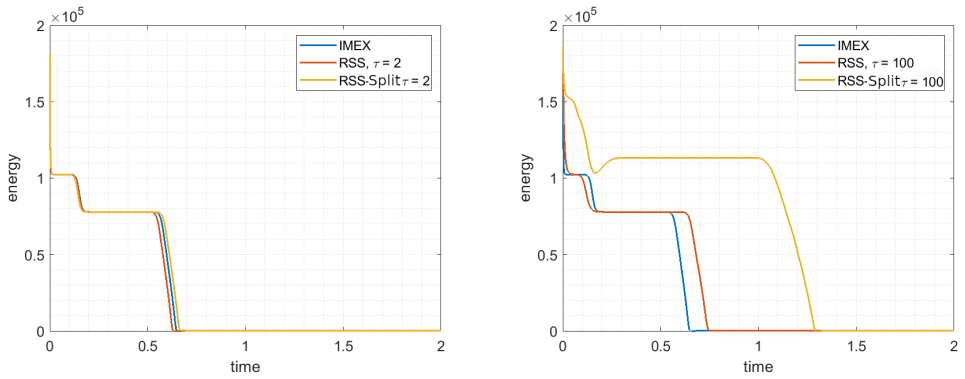

Figure 10: History of the numerical energy for the 3D Allen-Cahn equation with different time schemes. The initial condition is $u_0(x, y, z) = \cos(\pi x)\cos(5\pi y)\cos(3\pi z)$. The parameters are $\varepsilon = 0.1$, $N = 16$, $\Delta t = 10^4$ and $\tau = 2$.

5.2.2 Image Segmentation

The RSS method is derived form the splitting scheme proposed in [26] (that we recover in the case $\tau = 1$ and $B = A$) and reads as

Algorithm 7 : RSS-splitting for Image segmentation with Allen Cahn

1: **for** $k = 0, 1, \cdots$ **do**

2: **Set**

$$c_1^{(k)} = \frac{\int_\Omega f_0(x)(1+\phi^{(k)}(x))dx}{\int_\Omega (1+\phi^{(k)}(x))dx}$$
$$c_2^{(k)} = \frac{\int_\Omega f_0(x)(1-\phi^{(k)}(x))dx}{\int_\Omega (1-\phi^{(k)}(x))dx}$$

3: **Solve** $\frac{\phi^{(k+1/3)}-\phi^{(k)}}{\Delta t} = -\lambda\left((1+\phi^{(k+1/3)})(f_0-c_1^{(k)})^2 - (1-\phi^{(k+1/3}(f_0-c_2^{(k)})^2\right)$

4: **Solve** $(Id + \tau\Delta t B)\delta\phi = -\Delta t A\phi^{(k+/3)}$

5: **Set** $\phi^{(k+2/3)} = \phi^{(k+1/3)} + \delta\phi$

6: **Set** $\phi^{(k+1)} = \frac{\phi^{(k+2/3)}}{\sqrt{e^{-2\frac{\Delta t}{\epsilon^2}} + (\phi^{(k+2/3)})^2(1-e^{-2\frac{\Delta t}{\epsilon^2}})}}$

7: **end for**

In our numerical experiments, the given image f is normalized with $f_0 = \frac{f - f_{min}}{f_{max} - f_{min}}$, where f_{max} and f_{min} are the maximum and the minimum values of the given image, respectively, so we have $f_0 \in [0, 1]$. The initial condition is $\phi = 2f_0 - 1$ and $\Omega =]0, 1[^2$.
We here apply a post-processing similar to the one described in section 4.2.1 for the inpainting problem to obtain sharp boundaries. The thresholded images are labelled *segmented image* while those computed at the final time t^* (then before thresholding) are labelled *segmented image at* $t = t*$. We observe in Figures 11 and 12 the segmentation process of two classical images: the results are satisfactory, they are in good agreement with those of the literature; the extremal values of the two phases are respectively very close to -1 and 1 during the time evolution and the convergence to the steady state (segmented image at a sufficient large given time) is linear; the iterations in time are stopped when the L^2 norm of the time derivative of the solution is smaller than $1.e-4$, the current numerical solution is then considered as a steady state.

We used Lele's compact schemes for the space discretization and used the 2 dimensional cosine FFT for the solution of the linear systems in the RSS schemes; similar results are obtained using CS2 compact scheme.

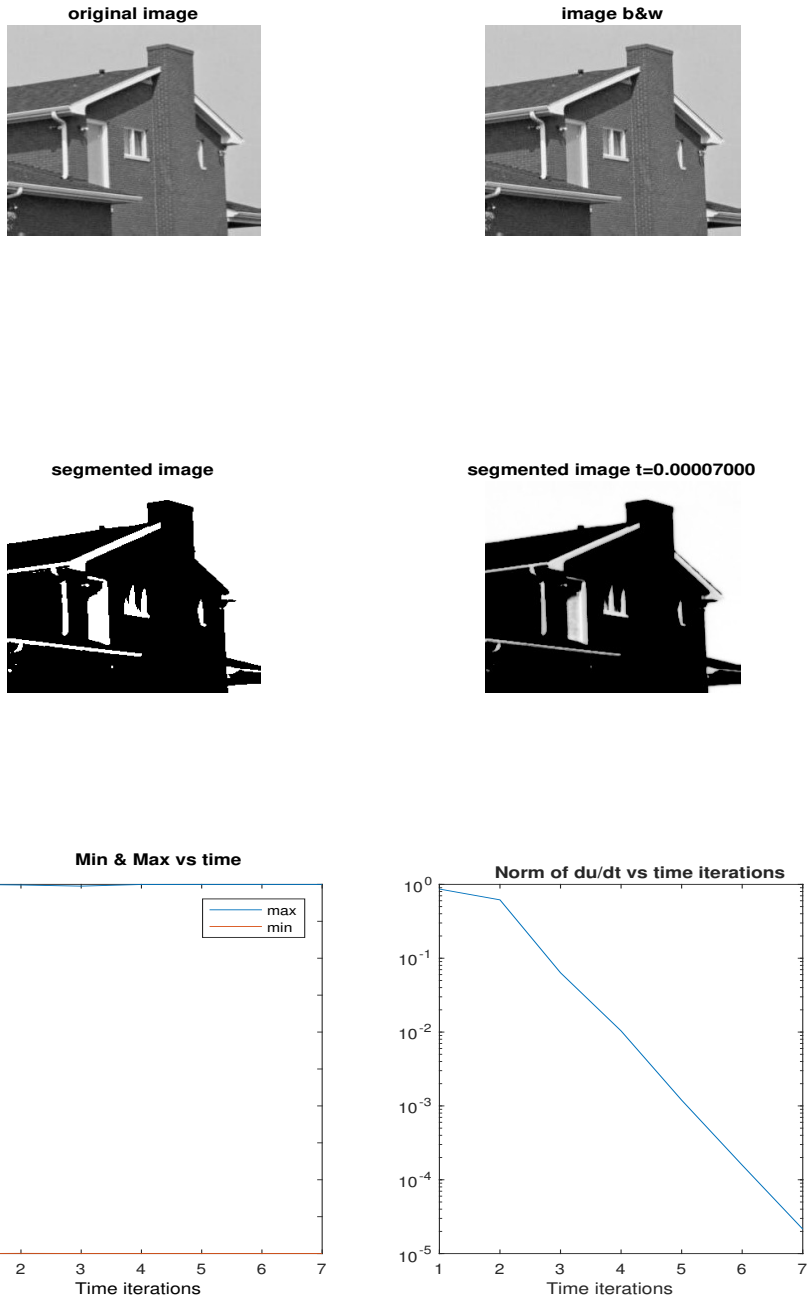

Figure 11: House image. On lines 1 and 2: from original image to its segmentation (with RSS scheme) $\Delta t = 1.e-5$, $\epsilon = 0.01$, $\tau = 1$, $\lambda = 10^{10}$. On line 3: min and max values vs time iterations (left) and L^2 norm of the discrete time derivative of the solution vs time iterations.

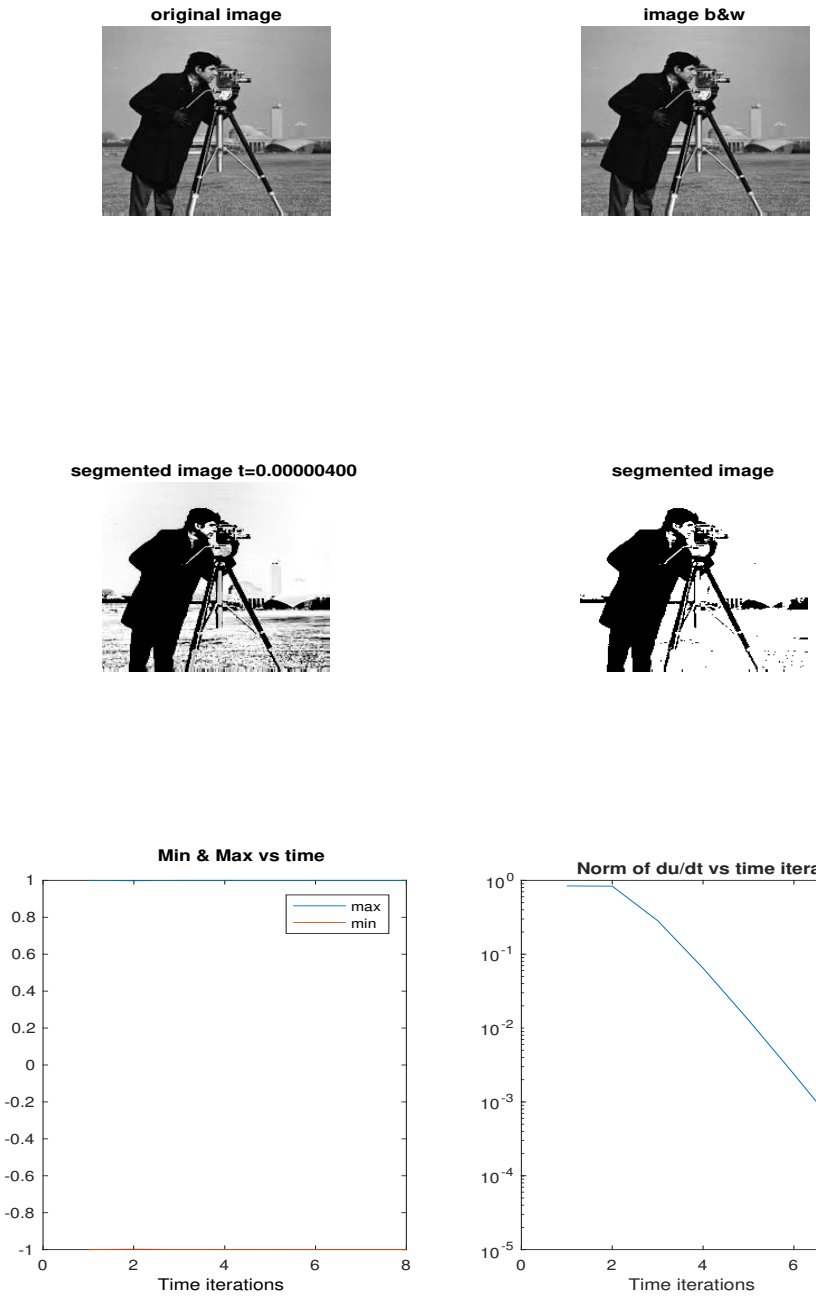

Figure 12: Cameraman image. On lines 1 and 2: from original image to its segmentation (with RSS scheme) $\Delta t = 5.e-7$, $\epsilon = 0.04$, $\tau = 1$, $\lambda = 10^{10}$. On line 3: min and max values vs time iterations (left) and L^2 norm of the discrete time derivative of the solution vs time iterations.

5.3 Cahn-Hilliard equation

5.3.1 Pattern Dynamics

As previously for the Allen-Cahn equation, we begin by comparing the computational time for each times schemes. The 2D then the 3D case are considered and reported in the following tables (3) and (4) respectively. We computed the CPU time for different values of N. It appears clearly that the stabilized schemes allow to obtain an important reduction of the CPU time and that this reduction increases as the dimension of the problem increases.

	IMEX	RSS ($\tau = 4$)	NLRSS ($\tau = 4$)
CPU time $N = 8$	0.4625	0.5289	1.1548
CPU time $N = 16$	2.3725	0.6118	1.6168
CPU time $N = 32$	26.641	1.2065	3.9783
CPU time $N = 64$	1592.0	14.723	65.072

Table 3: 2D Cahn-Hilliard equation. Final time $t_{\max} = 0.01$, $\Delta t = 10^{-5}$, $\varepsilon = 0.05$. CPU time in seconds.

	IMEX	RSS ($\tau = 4$)	NLRSS ($\tau = 4$)
CPU time $N = 8$	26.056	0.8668	2.6006
CPU time $N = 16$	2415.1	6.8601	71.052
CPU time $N = 32$	too long.	84.045	1287.9

Table 4: 3D Cahn-Hilliard equation. Final time $t_{\max} = 0.1$, $\Delta t = 10^{-4}$, $\varepsilon = 0.05$. CPU time in seconds.

In the results presented below, we used CS2 Compact Schemes discretization in space and the 2D then the 3D cosine FFT for a fast solution of the linear systems arising in RSS-schemes.

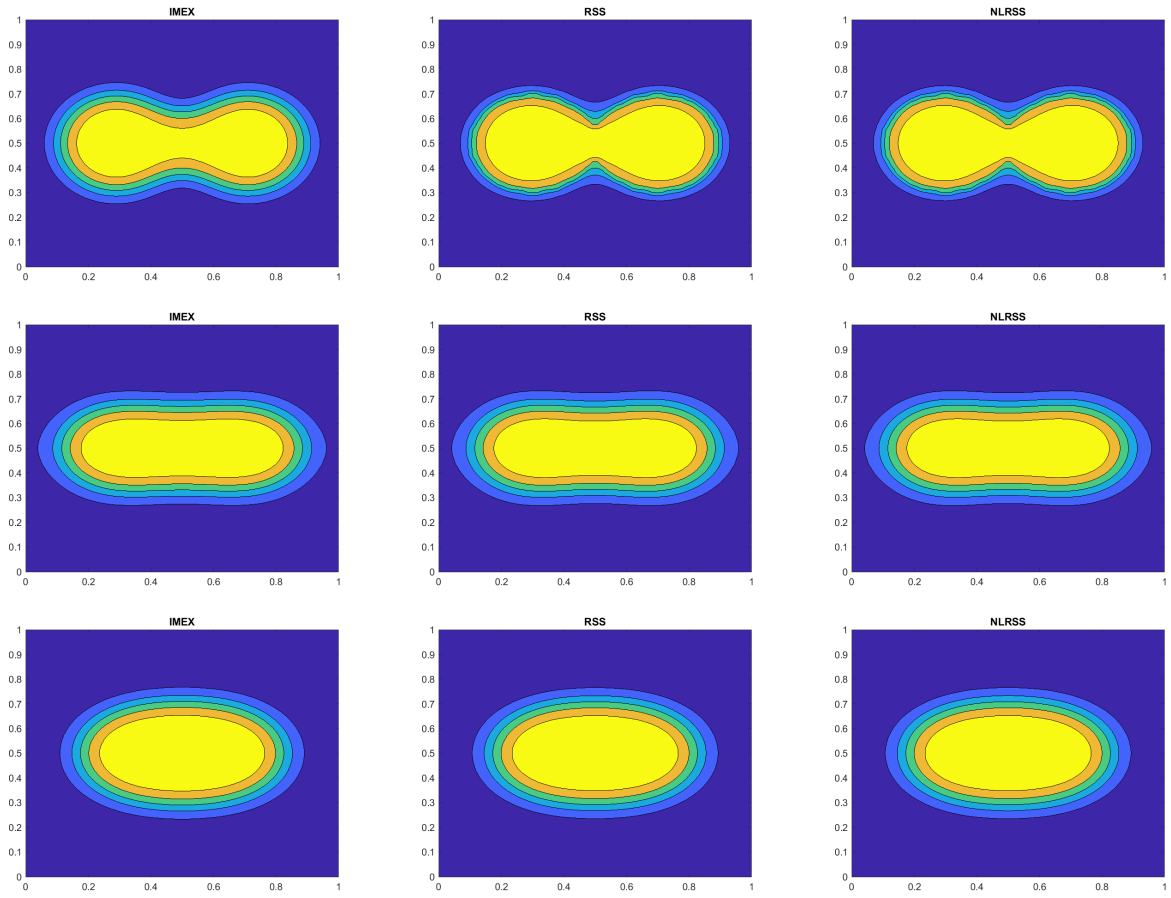

Figure 13: Solution of the 2D Cahn-Hilliard equation with different time schemes. The initial condition is given by two circles. Line by line, the numerical solution are at time $t = 10^{-4}$, $t = 10^{-3}$ and $t = 5 \cdot 10^{-3}$. The parameters are $\varepsilon = 0.05$, $N = 64$, $\Delta t = 10^{-5}$ and $\tau = 4$.

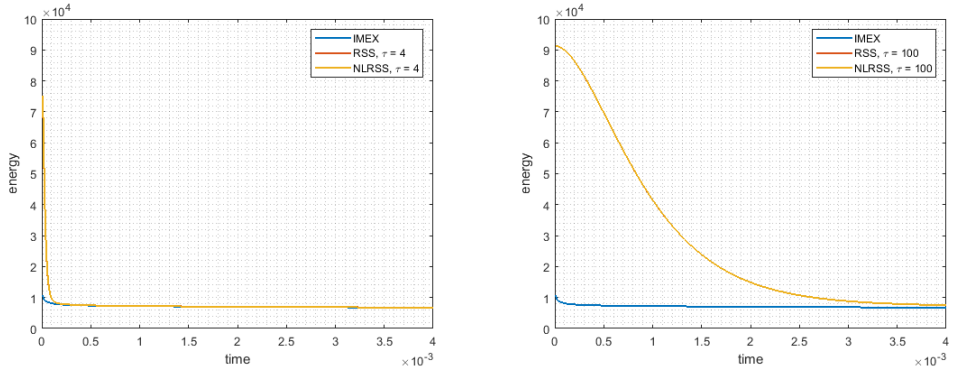

Figure 14: History of the numerical energy for the 2D Cahn-Hilliard equation with different time schemes. The initial condition is given by two circles. Line by line, the numerical solution are at time $t = 10^{-4}$, $t = 10^{-3}$ and $t = 5 \cdot 10^{-3}$. The parameters are $\varepsilon = 0.05$, $N = 64$, $\Delta t = 10^{-5}$ and $\tau = 4$.

We consider now the pattern dynamics problem in 3D:

$$\frac{\partial u}{\partial t} - \Delta(-\epsilon\Delta u + \frac{1}{\epsilon}f(u)) = 0, \quad x \in \Omega =]0,1[^3, \tag{73}$$

$$\frac{\partial u}{\partial n} = 0, \frac{\partial}{\partial n}\left(\Delta u - \frac{1}{\epsilon^2}f(u)\right) = 0, \tag{74}$$

$$u(0,x) = u_0(x). \tag{75}$$

We now compare the 3 schemes IMEX, NLRSS and IMEX-RSS for a given deterministic initial datum $u_0(x,y,z) = \cos(\pi x)\cos(2\pi y)\cos(3\pi z)$: as shown in Figure 15, RSS-IMEX capture the pattern dynamics with a decreasing energy and a conserved null mean value of the solution. In Figure 16 we compare the time evolution of the energy for the 3 schemes when taking $\tau = 4$, then $\tau = 100$. We can observe here clearly the rule of τ: the stabilization can slow down the dynamics when large values of τ are taken: the choice $\tau = 4$ allow the RSS scheme to have their time evolution of the energy comparable to that of the reference scheme while when $\tau = 100$, the RSS schemes converge much more slowly to the global minimizer.

5.3.2 Inpainting

We consider here the inpainting problem (see e.g. [6, 7, 11])

$$\frac{\partial u}{\partial t} - \Delta(-\epsilon\Delta u + \frac{1}{\epsilon}f(u)) \quad + \lambda\chi_{\Omega\setminus D}(x)(u-g) = 0, \tag{76}$$

$$\frac{\partial u}{\partial n} = 0 \quad \frac{\partial}{\partial n}\left(\Delta u - \frac{1}{\epsilon^2}f(u)\right) = 0, \tag{77}$$

$$u(0,x) = u_0(x), \tag{78}$$

described in the previous section. Here $\Omega =]0,1[^2$, the schemes used is RSS-IMEX for inpainting (Algorithm 6). We proceed following the approach described in Section 4.1 and used in [11]:

- At first, for fixed $\epsilon > 0$, we compute the solution up to a converged time t^* (here $t^* = 6 \times 10^{-3}$).
- Then, we apply a post-processing consisting in a thresholding which replaces the dominant phase by 1 at every point of Ω and the other phases (colors) by 0. The final result exhibit sharp contrasts, as we can see in Figures 17 and 18.

We here used CS2 Compact Schemes discretization in space. However the implicit par in the RSS scheme is not particularly adapted to the use of cosine FFT: this is to the presence of the linear fidelity operator. The linear systems are solved using the *backslash* command \.

The results agree with the ones presented in the inpainting problem (see e.g. [11]).

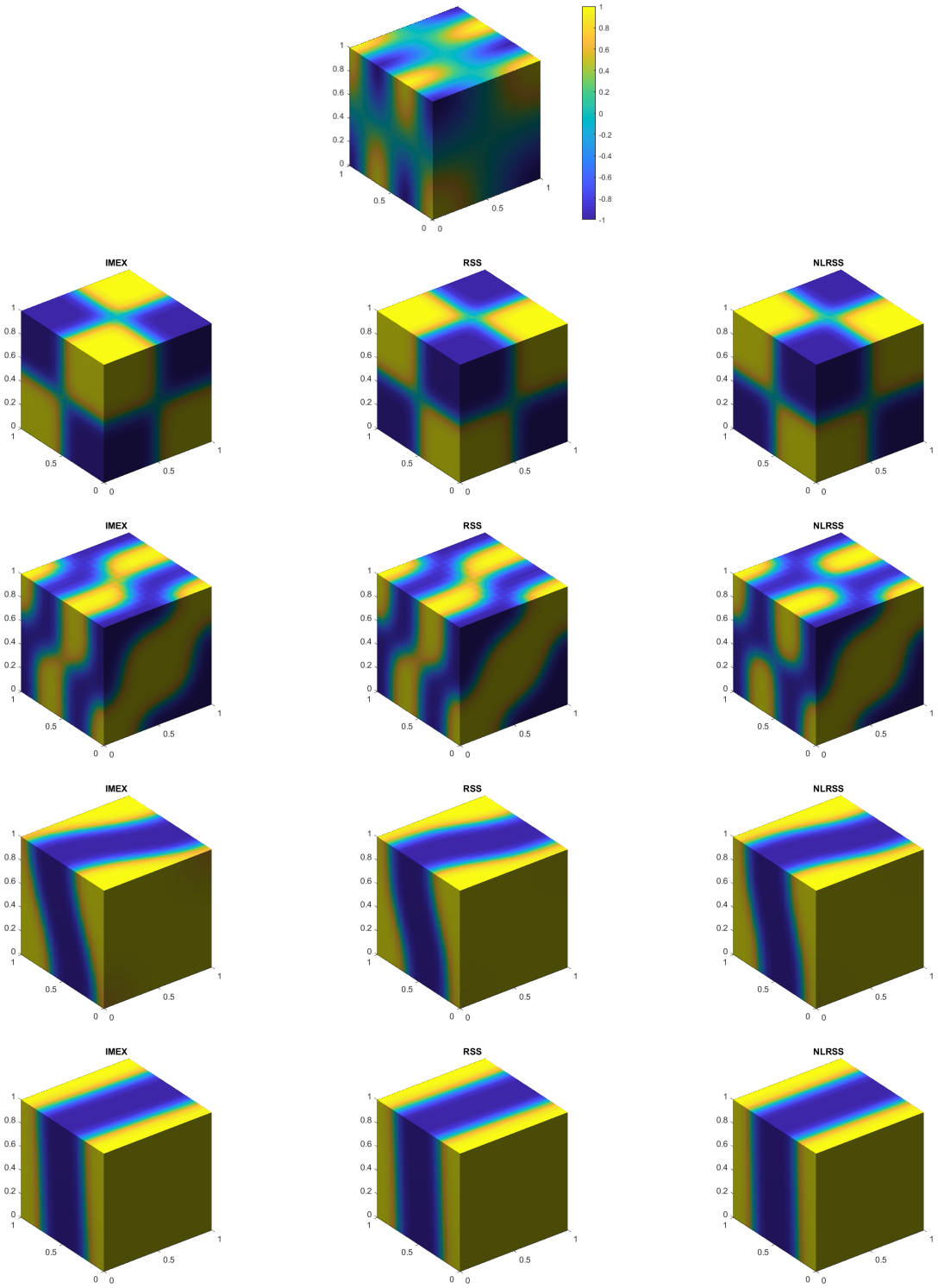

Figure 15: Solution of the 3D Cahn-Hilliard equation with different time schemes. The initial condition is given by $u_0(x, y) = \cos(2\pi x)\cos(2\pi y)\cos(\pi z)$. Line by line, the numerical solution are at time $t = 0$, $t = 0.03$, $t = 0.05$, $t = 0.07$ and $t = 0.1$. The parameters are $\varepsilon = 0.05$, $N = 16$, $\Delta t = 10^{-4}$ and $\tau = 4$.

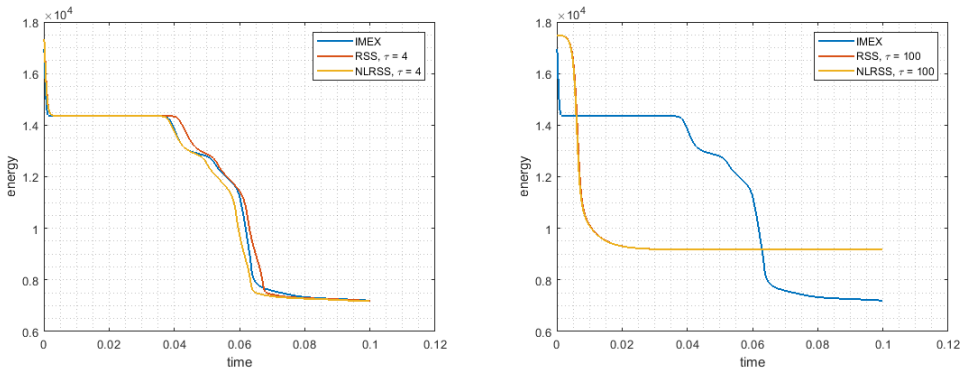

Figure 16: History of the numerical energy for the 3D Cahn-Hilliard equation with different time schemes. The initial condition is $u_0(x, y) = \cos(2\pi x)\cos(2\pi y)\cos(\pi z)$. The parameters are $\varepsilon = 0.05$, $N = 16$ and $\Delta t = 10^{-4}$.

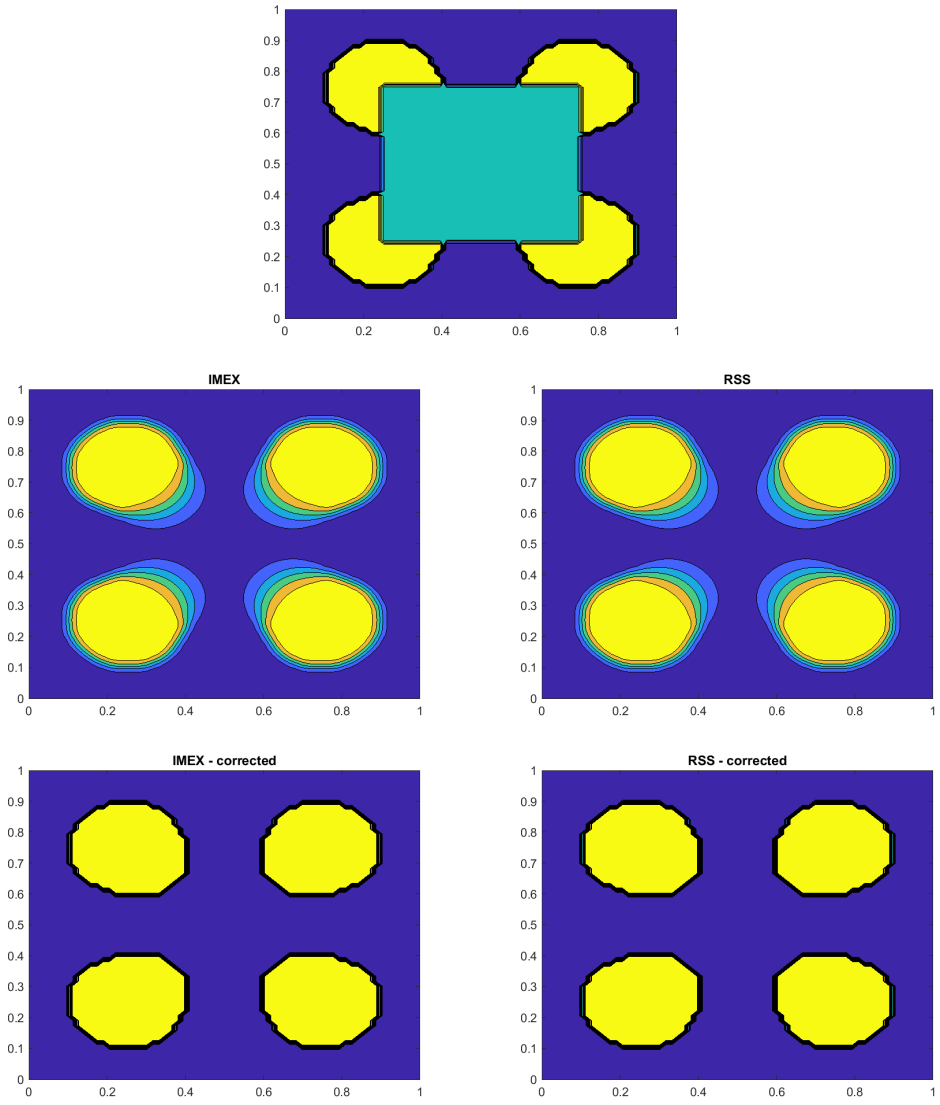

Figure 17: Inpainting using the Cahn-Hilliard equation. The PDEs parameter are $\varepsilon = 0.05$ and $\lambda = 900000$. The numerical parameters are $N = 64$, $\Delta t = 10^{-6}$ and $\tau = 4$ (for RSS scheme). The final time is $t = 5 \cdot 10^{-3}$. Top : initial map. The blue square represents the inpainting area. Center line : solution with IMEX (left) and RSS (right) scheme at final time. Bottom line : solution at final time with IMEX (left) and RSS (right) scheme after correction.

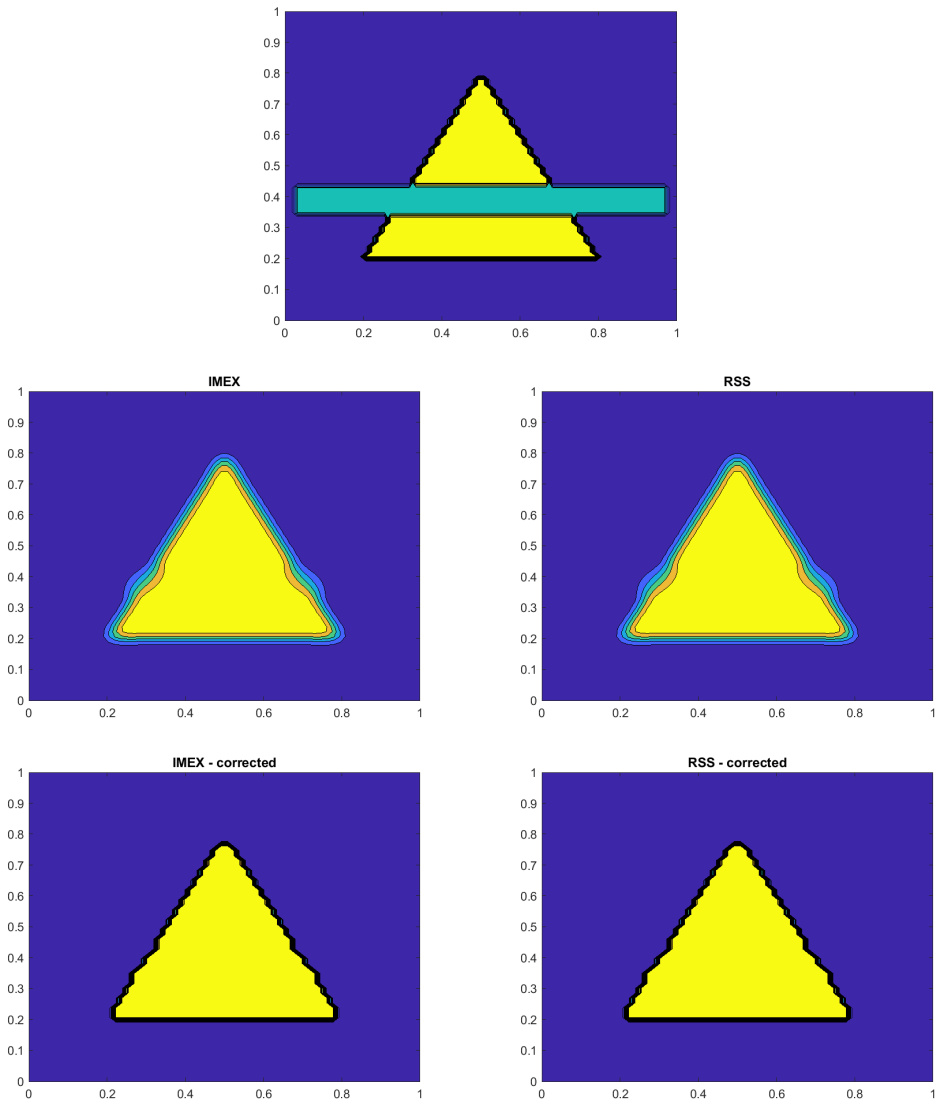

Figure 18: Inpainting using the Cahn-Hilliard equation. The PDEs parameter are $\varepsilon = 0.05$ and $\lambda = 900000$. The numerical parameters are $N = 64$, $\Delta t = 10^{-6}$ and $\tau = 4$ (for RSS scheme). Results are given after 100 iterations. Top : initial map. The blue rectangle represents the inpainting area. Center line : solution with IMEX (left) and RSS (right) scheme at final time. Bottom line : solution at final time with IMEX (left) and RSS (right) scheme after correction.

6 Concluding remarks and perspectives

We have introduced stabilized finite differences semi-implicit schemes that allow a fast simulation of high accurate solutions of phase fields problems since the main effort of the computation lies on the efficient solution of sparse linear systems. These new time marching scheme allow to use computational facilities of the sparse linear algebra and also of the fast solvers, depending on the situation. We have considered only finite differences but the use of two different levels of accuracy can be applied to other discretization techniques, such as finite elements. Of course several questions have still to be considered and we address to future work the following possible developments:

- The stabilization procedure has been here applied to simple IMEX schemes, but it is versatile and can be considered together with other time marching schemes. Indeed, it can apply also to accelerate the diffusion parts of the numerical solution of gradient flows by SAV-like schemes, recently studied, eg, in [35]. These schemes are obtained by introducing the discretization of the auxiliary variable $s(t) = \sqrt{\int_\Omega F(u)dx + C_0}$ and adding the time-derivative of this last expression to avoid the implicitly; here C_0 is a positive constant chosen such that $F(u) + C_0 > 0, \forall u$.
  The IMEX-scheme applied to the discretized Cahn-Hilliard system reads as

$$\frac{u^{(k+1)} - u^{(k)}}{\Delta t} + A\mu^{(k+1)} = 0, \tag{79}$$

$$\mu^{(k+1)} = Au^{(k+1)} + \frac{s^{(k+1)}}{\sqrt{Q_h(F(u^{(k)})) + C_0}} f(u^{(k)}) = 0, \tag{80}$$

$$\frac{s^{(k+1)} - s^{(k)}}{\Delta t} = Q_h\left(\frac{f(u^{(k)})}{2\sqrt{Q_h(F(u^{(k)})) + C_0}} \frac{u^{(k+1)} - u^{(k)}}{\Delta t}\right) \tag{81}$$

  Here, the expression $Q_h(v)$ corresponds to a quadrature formula applied to v: $Q_h(v) \simeq \int_\Omega v dx$. This scheme is unconditionally stable for the modified energy

$$E_{SAV}(u, s) = \frac{1}{2} Q_h(< Au, u >) + s^2,$$

  that means that $E_{SAV}(u^{(k+1)}, s^{(k+1)}) \leq E_{SAV}(u^{(k)}, s^{(k)}), \forall k \geq 0, \ \forall \Delta t > 0$, see [35]. The derivation of the stabilized IMEX-SAV scheme simply writes as

$$\frac{u^{(k+1)} - u^{(k)}}{\Delta t} + \tau B(\mu^{(k+1)} - \mu^{(k)}) = -A\mu^{(k)}, \tag{82}$$

$$\mu^{(k+1)} - \mu^{(k)} = \tau B(u^{(k+1)} - u^{(k)}) + Au^{(k)} - \mu^{(k)} + \frac{s^{(k+1)}}{\sqrt{Q_h(F(u^{(k)})) + C_0}} f(u^{(k)}), \tag{83}$$

$$\frac{s^{(k+1)} - s^{(k)}}{\Delta t} = Q_h\left(\frac{f(u^{(k)})}{2\sqrt{Q_h(F(u^{(k)})) + C_0}}, \frac{u^{(k+1)} - u^{(k)}}{\Delta t}\right). \tag{84}$$

  We can obtain the following stability result combining the proof of Theorem 4.1 and that of the stability of the SAV scheme as presented in [35]:

Proposition 6.1 *Under the hypothesis of Theorem 4.1, we have the following stability conditions: If* $\tau \geq max(\beta, \frac{L}{2\epsilon^2 \lambda_{min}(B)} + \frac{\beta}{2})$, *then the scheme (82) - (84) is unconditionally stable for the modified energy* E_{SAV}. *Here* $\lambda_{min}(B) > 0$ *is the smallest strictly positive eigenvalue of* B. *In addition,* $u^{(k+1)} - u^{(k)} \in W^\perp, \forall k \geq 0$, *where* $W = Ker(A) = Ker(B)$, *in particular, if* $W = \{\mathbf{1}^T\}$, *the mean value of* $u^{(k)}$ *is conserved.*

Proof. We set for simplicity $Q_h(g) = \sum_\ell g_\ell h^d$, where d is the dimension of Ω and ℓ the multi-index coordinate of the array g_ℓ containing the approximation of g at the grid points. We take $Q_h(< \mu^{(k+1)}, (82) >)$ then $Q_h(< u^{(k+1)} - u^{(k)}, (83) >)$. Using both the same majorations as in the proof of Theorem 4.1 and the identity

$$s^{(k+1)} Q_h \left(\frac{f(u^{(k)})}{\sqrt{Q_h(F(u^{(k)})) + C_0}}, u^{(k+1)} - u^{(k)} \right) = |s^{(k+1)}|^2 - |s^{(k)}|^2 + |s^{(k+1)} - s^{(k)}|^2,$$

we obtain the result. ■

- The key point in our methods is the choice of the preconditioning matrix B and of the tuning stabilization parameter τ, the stabilization matrix being here defined as $B_\tau = \tau B$. In an ideal situation, the stabilization should only act on the high mode components of the solution: indeed, their speed of propagation determines the time step restriction. Also a strong stabilization of the low mode components of the solution can slow down the dynamics, see [1]; this typically arises when taking large values of τ, as also illustrated in the present work for Allen-Chan's or Cahn-Hilliard's pattern dynamics. In our situation, i.e, when considering two finite differences discretisations A and B of the same operator, typically $-\Delta$, the lower eigenvalues of B are very close to those of A while the high ones are underestimated as respected to the A's ones, see Section 2.4 and more generally [25]. So, when $\tau \simeq 1$, τB stabilizes the IMEX-scheme without deteriorating the consistency. To enhance much more significantly the stabilization, one faces to the construction of a preconditioner B_τ whose the spectrum is close to the one of A for the small eigenvalues and which controls the high eigenvalues for large values of τ. This question adresses to linear algebra techniques, see e.g. [32, 33].

References

[1] H. Abboud, C. Al Kosseifi and J.-P. Chehab, A Stabilized bi-grid method for Allen-Cahn equation in Finite Elements. Computational and Applied Mathematics,(2019) 38: 35. https://doi.org/10.1007/s40314-019-0781-0

[2] S. M. Allen, J. W. Cahn. Ground State Structures in Ordered Binary Alloys with Second Neighbor Interactions. Acta Met. 20, 423 (1972).

[3] S. M. Allen, J. W. Cahn. A Correction to the Ground State of FCC Binary Ordered Alloys with First and Second Neighbor Pairwise Interactions. Scripta Met. 7, 1261 (1973).

[4] A. Averbuch, A. Cohen and M. Israeli, A stable and accurate explicit scheme for parabolic evolution equations. rapport LAN (1998), unpublished.

[5] M. Benes, V. Chalupecky, K. Mikula, Geometrical image segmentation by the Allen-Cahn equation, Applied Numerical Mathematics 51, (2004), 187-205.

[6] A. Bertozzi, S. Esedoglu, and A. Gillette, Analysis of a two-scale Cahn–Hilliard model for binary image inpainting, Multiscale Model. Simul. 6 (2007), 913–936.

[7] A. Bertozzi, S. Esedoglu, and A. Gillette, Inpainting of binary images using the Cahn- Hilliard equation, IEEE Trans. Image Proc. (2007), 285–291.

[8] M. Brachet, J.-P. Chehab, Stabilized Times Schemes for High Accurate Finite Differences Solutions of Nonlinear Parabolic Equations, of Scientific Computing, 69 (3) (2016), 946–982.

[9] C. Bolley, Solutions numériques de problèmes de bifurcation ESAIM: Mathematical Modelling and Numerical Analysis - Modélisation Mathématique et Analyse Numérique, Tome 14 (1980) no. 2, p. 127–147.

[10] J.-P. Chehab, A.A. Franco and Y. Mammeri, Boundary Control of the number of the interfaces for the one-dimensional Allen-Cahn equation, DiscR. Cont. dyn. Syst. Serie S, Volume 10, Number 1 (2017), 87–100.

[11] L. Cherfils, H. Fakih, and A. Miranville, On the Bertozzi-Esedoglu-Gillette-Cahn- Hilliard equation with logarithmic nonlinear terms, SIAM J. Imag. Sci 8 (2015), 1123–1140.

[12] B. Costa. L. Dettori, D. Gottlieb and R. Temam, Time marching techniques for the nonlinear Galerkin method, SIAM J. SC. comp., 23, (2001), 1, 46–65.

[13] L. Collatz, *The Numerical Treatment of Differential Equations*, 3rd Edition, Springer-Verlag, (1966).

[14] A. E. Diegel, *Numerical Analysis of Convex Splitting Schemes for Cahn-Hilliard and Coupled Cahn-Hilliard- Fluid-Flow Equations*, PhD thesis, may 2015, University of Tennessee - Knoxville

[15] D. Dutykh. How to overcome the Courant-Friedrichs-Lewy condition of explicit discretizations? Technical Report, 20 pp, 2016, `https://hal.archives-ouvertes.fr/hal-01401125/document`

[16] S. Gasparin, J. Berger, D. Dutykh, N. Mendes. Stable explicit schemes for simulation of nonlinear moisture transfer in porous materials, J. of Build. Perf. Sim., (2017), Volume 11, 2018 - Issue 2, pp 129–144.

[17] C.M. Elliott, The Cahn-Hilliard Model for the Kinetics of Phase Separation, *in Mathematical Models for Phase Change Problems*, International Series of Numerical Mathematics, Vol. 88, Birkhäuser, (1989).

[18] C.M. Elliott and A. Stuart The global dynamics of discrete semi-linear parabolic equations. SIAM J. Numer. Anal. 30 (1993) 1622–1663.

[19] H. Emmerich, *The Diffuse Interface Approach in Materials Science Thermodynamic. Concepts and Applications of Phase-Field Models.* Lecture Notes in Physics Monographs, Springer, Heidelberg, (2003).

[20] D. J. Eyre, Unconditionallly Stable One-step Scheme for Gradient Systems, June 1998, unpublished, http://www.math.utah.edu/eyre/research/methods/stable.ps.

[21] H. Fakih, *Etude mathématique et numérique de quelques généralisations de l'équation de Cahn-Hilliard : Applications à la retouche d'images et à la biologie*, Doctoral Thesis, University of Poitiers, (december 2014).

[22] J. Jiang, J. Shi. *Bistability Dynamics in Structured Ecological Models. Spatial Ecology*, Stephen Cantrell, Chris Cosner, Shigui Ruan ed., CRC Press, (2009).

[23] Kokiopoulou and Y. Saad. , *Orthogonal Neighborhood Preserving Projections*, Proc. ICDM05, J. Han et al. ed., IEEE, pp. 234–241 (2005).

[24] D. Lee , J-Y Huh , D. Jeong , J. Shin, A.Yun a J. Kim, Physical, mathematical, and numerical derivations of the Cahn-Hilliard equation. Computational Materials Science 81 (2014) 216–225.

[25] S. Lele, Compact Difference Schemes with Spectral Like resolution, J. Comp. Phys., 103, (1992), 16–42.

[26] Y. Li, H. G. Lee, D. Jeong, J. Kim, An unconditionally stable hybrid numerical method for solving the Allen-Cahn equation, Computers and Mathematics with Applications 60 (2010), 1591–1606.

[27] Y. Li, D. Jeong, J. Choi, S. Lee, J. Kim, Fast local image inpainting based on the Allen-Cahn model, Digital Signal Processing, 37 (2015), 65–74.

[28] B. Merlet, M. Pierre, Convergence to equilibrium for the backward Euler scheme and applications, Communications on Pure and Applied Analysis 9(3): 685–702 (2010).

[29] K.M. Morton and D.F. Mayers, *Numerical Solution of Partial Differential Equations: An Introduction*, Cambridge University Press, second Edition (2005)

[30] M. Pierre and A. Rougirel, Stationary solutions to phase field crystal equations, Math. Methods Appl. Sci., 34 (2011), no. 3, pp. 278–308.

[31] N. Provatas and K. Elder, *Phase-Field Methods in Material Science and Engineering*, Wiley-VCH

[32] Y. Saad *Numerical Methods for Large Eigenvalue Problems* SIAM, 2011, second Edition.

[33] Y. Xi and Y. Saad. Fast computation of spectral densities for generalized eigenvalue problems. SIAM J. Sci. Comput., 40(4) (2018), 2749–2773.

[34] J. Shen, X. Yang, Numerical Approximations of Allen-Cahn and Cahn-Hilliard Equations. DCDS, Series A, (28), (2010), pp 1669–1691.

[35] Jie Shen, Jie Xu and Jiang Yang, A New Class of Efficient and Robust Energy Stable Schemes for Gradient Flows, SIAM Rev., 61(3), (2019), 474–506.

[36] G. Strang, The DIscrete Cosine Transform, SIAM Review,1999, Vol. 41, No. 1, pp. 135–147.

[37] R. Temam, *Infnite-dimensional dynamical systems in mechanics and physics*, 2nd Ed., Springer-Verlag, New York, 1997.